

A Comparison and Catalog of Intrinsic Tumor Growth Models

E.A. Sarapata^{a,1,**}, L.G. de Pillis^{a,*}

^a*Department of Mathematics, Harvey Mudd College, Claremont, CA 91711*

Abstract

Determining the mathematical dynamics and associated parameter values that should be used to accurately reflect tumor growth continues to be of interest to mathematical modelers, experimentalists and practitioners. However, while there are several competing canonical tumor growth models that are often implemented, how to determine which of the models should be used for which tumor types remains an open question. In this work, we determine the best fit growth dynamics and associated parameter ranges for ten different tumor types by fitting growth functions to at least five sets of published experimental growth data per type of tumor. These time-series tumor growth data are used to determine which of the five most common tumor growth models (exponential, power law, logistic, Gompertz, or von Bertalanffy) provides the best fit for each type of tumor.

Keywords: Population dynamics, Parameter fitting, Dynamical systems

1. Introduction

Intrinsic tumor growth functions are a component of nearly all continuous, deterministic, cell-population based cancer models, yet there is no universal consensus as to which intrinsic growth function should be used when a new mathe-

*Corresponding author

**Principal corresponding author

Email addresses: esarapata@hmc.edu (E.A. Sarapata), depilllis@hmc.edu (L.G. de Pillis)

¹Telephone: 917-216-0573. This author has no affiliations or conflicts of interest.

mathematical model is being built. Of the published works which focus exclusively on intrinsic tumor growth, five models are widely used: exponential growth functions, power Law functions, logistic growth functions, von Bertalanffy growth functions, and Gompertz growth functions [1, 2]. In a study by Hart *et al.*[2], the authors compare Gompertz, logistic, exponential and power law growth against mammography data on human breast cancer. The authors ultimately conclude that the power law should be used to represent breast cancer growth, though future investigations by the same authors found logistic growth to yield a better fit to the data of interest [2, 3]. Another study by de Pillis and Radunskaya, in which intrinsic tumor growth functions for murine melanoma were compared, concluded that von Bertalanffy and logistic growth models provided the most accurate fit to data [1]. A study by Zheng *et al.* [4] compares exponential and biexponential models of lung cancer growth, in which the biexponential model is meant to approximate a tumor with two different speeds of growth. That study concludes that a biexponential model produces a better fit in all tested cases.

The choice of intrinsic growth function is strongly driven by the type of cancer being modeled, in addition to the environment in which it is growing (*e.g.*, in vitro, in mice, or in humans). In this work, we carry out a thorough exploration of a large collection of published cancer growth data in both mice and humans, and determine the best fit intrinsic growth functions along with the associated parameter ranges. For each of the ten tumor types we analyze, we have collected between five and ten separate sets of experimental data. After normalizing the data sets so they can be compared, we fit the data to exponential, power law, logistic, Gompertz and von Bertalanffy growth models.

The process of comparing different growth functions to data naturally yields biologically relevant parameter values and ranges associated with each function. We provide all those parameter ranges in this work. Mathematical modelers must often be creative in choosing appropriate model parameters: they may borrow parameter values directly from published sources, or they may fit functions to data, if relevant data are available, or they may just have to use an *ad*

hoc value, choosing a value that yields biologically reasonable dynamics. A large number of studies use experimental data from radically different experiments to estimate parameters; it is nearly unavoidable to combine data from murine and human sources, or obtained from *in vitro* and *in vivo* trials [5, 6, 7, 8]. The challenge of function choice and parameter determination will always be present for the modeler, and techniques for case-by-case parameter choice will still have to be pursued [9]. However, the catalog of intrinsic growth laws and associated parameter ranges we provide for a variety of commonly modeled cancer types should provide a helpful starting point as researchers develop new models.

2. Assumptions and Methods

2.1. Experimental data

We curated time series tumor growth data sets for ten types of tumor: bladder cancer, breast cancer, colon cancer, head and neck squamous cell carcinoma, hepatocellular carcinoma, lung cancer, melanoma, ovarian cancer, pancreatic cancer, and renal cell carcinoma. Each group of data sets was collected from at least five peer-reviewed publications, with the smallest-sized group containing seven data sets and the largest containing seventeen data sets. In addition, at least one data set collected for each type of cancer was obtained from *in vitro* trials and at least one data set was collected from *in vivo* trials. Along with *in vitro* trials, the range of target organisms included SCID mice, nude mice, normal mice, hamsters and humans. Table Appendix B.1 shows all sources for each time series data set included in our study, as well as the cell lines for each trial.

2.2. Unit normalization

Among the publications that reported time series tumor growth data, the units and methods of tumor size measurement varied greatly. At least one paper per type of tumor was an *in vitro* trial that reported tumor size as a cell number, the preferred unit for our purposes, but all data from *in vivo*

and *in situ* trials were presented in units of mm^3 , mm^2 , mm , cm^3 , or relative volume. A study by Dempsey *et al.* demonstrated that unidimensional and bidimensional measures of tumor growth are less accurate as a predictor of survival than volumetric measures, leading to a possible source of pre-analytic error [10]. In addition, instead of assuming a spherical tumor, volume was reported in a majority of papers as the product of the height, length and width of the tumor, overestimating the volume. However, we will also assume that no individual tumor cells are compressed, which will underestimate the number of tumor cells. The combination of these two assumptions is presumed to bring the estimated cell number within reasonable error of the real cell number.

In many cases, we were able to obtain an estimate of the number of tumor cells in a given volume from murine data sets that reported an initial cell count along with an initial volume measurement. We then divided the volume by the cell number, allowing for an estimate of the volume of a single tumor cell. We used this same estimate for data sets on tumor growth for tumors originating from the same organ. The most accurate conversion estimate, requiring the fewest conversions from the original data, was an estimate of $2.85 \times 10^3 \text{ cells}/\mu\text{m}^3$ for pancreatic cancer [11]. For types of tumor that did not have a conversion data set available, we estimated the conversion ratio at approximately $1.82 \times 10^3 \text{ cells}/\mu\text{m}^3$ [6]. Although these two estimates were obtained from different sources and for different cells, it should be noted that they are the same order of magnitude despite the high variability of cell size.

This volume estimate of a tumor cell provides a method with which to convert volume, area or length measurements to cell number. For those data sets which reported growth in volume, we normalized each datum by $\frac{1}{\mu_T}$ where μ_T is the tumor cell volume calculated as above. All of the publications that reported an area measurement obtained values by multiplying the minor axis of the tumor by the major axis [12, 13, 14, 15]. In this case, we assumed a cubic tumor with a volume of $a\sqrt{a}$ where a is the reported area measurement. This allows us to calculate cell number from volume as before. Another set of papers reported only the major axis of the tumor [16, 17, 18]. Here, we assumed a

spherical tumor with the radius being one-half the major axis, using the volume of the sphere to estimate the cell number. For those papers that reported relative volume, we converted the data to cell number using the information in the supplemental material sections of each paper [19, 20, 21].

2.3. ODE Tumor Growth Models

We compare fittings of tumor data for five different ODE growth models; exponential, power Law, logistic, Gompertz, and von Bertalanffy. Let P represent an arbitrary population and let t represent time. Exponential growth models are the simplest ODE growth model, described by

$$\frac{dP}{dt} = rP \quad (1)$$

for some intrinsic growth rate constant r . Exponential growth is actually a special case of power law growth, represented by

$$\frac{dP}{dt} = rP^a, \quad (2)$$

where both r and a are parameters that must be fit to the data. Logistic growth, which incorporates a population carrying capacity, is given by

$$\frac{dP}{dt} = rP \left(1 - \frac{P}{K}\right) \quad (3)$$

where r represents the intrinsic growth rate and K represents the carrying capacity. Logistic growth looks very much like exponential growth at low populations, but accounts for the resource-limited slowing of growth for larger populations. Von Bertalanffy growth, also incorporating a carrying capacity, is given by

$$\frac{dP}{dt} = r(K - P). \quad (4)$$

The final commonly used tumor growth model we will include is Gompertz growth, one form of which is given by

$$\frac{dP}{dt} = r \log\left(\frac{K}{P}\right) P. \quad (5)$$

Unfortunately, very few data sets track tumor growth long enough to sufficiently estimate carrying capacities. In order to get a good estimate, therefore, we sought out data sets that recorded large tumor cell populations, and compared the former two models against the latter three [20, 22, 16, 23, 11, 24, 25, 26, 12].

2.4. Parameter fitting algorithms

The parameters for each tumor growth model were estimated using at least two least-squares distance minimization algorithms. For each ODE model, the ODE with parameters was solved numerically using MATLAB's `ode45` function, which adaptively implements a 4th or 5th order Runge-Kutta solver. We then minimized a least squares distance function between the numerical ODE solution and a target set of data using either MATLAB's built-in `fminsearch` function or a Markov chain fitting with simulated annealing. MATLAB's `fminsearch` is a Nelder-Mead simplex direct search function. Nelder-Mead is one of a class of local-search algorithms. Local algorithms require that the user provide an initial value sufficiently close to the sought after solution, or the method may converge to nearby local minimum, but not to a global minimum. The local minimum found may not produce the best fit [27]. This necessitates the use of an alternate global data fitting method.

The global data fitting method we implement is a Markov chain Monte Carlo (MCMC) fitting with simulated annealing, a non-deterministic search algorithm. MCMC evaluates a wider range of values in parameter space than does `fminsearch`, and also includes a method for escaping from a local minimum to continue to search for a global minimum [28, 29, 30]. The stochasticity in the algorithm yields different outcomes even among trials with the same initial conditions [28, 29, 30]. The process is repeated n times, where n is an arbitrary number chosen by the user. The algorithm has no standard stopping condition. In our case, we chose $n = 200$. This number of runs allowed us to achieve relatively good fits while keeping computational running times reasonable. Implementing the algorithm with a larger number of iterations n may increase the chance that a global minimum is located.

Simulated annealing is the process of fitting, not to the distance function, but to the distance function raised to successive powers from 0 to 1, where the result of each fitting is used as the initial condition for the next fitting. The simulated annealing step reduces the chance that a minimization function will converge to a local minimum instead of a global minimum, since the act of raising the distance function to a power less than 1 reduces the prominence of local minima [28]. In our fittings, we ran 10 trials with simulated annealing, corresponding to ten iterations. Each iteration of the simulated annealing process involved n repetitions of MCMC, where, as above, $n = 200$.

While the local search algorithm `fminsearch` will return parameter values that produce the lowest least-squares fitting within a bounded neighborhood of the initial parameters, Markov chain methods such as MCMC return the parameter values that produce the lowest least-squares fitting over a finite number of arbitrary parameters from anywhere in the parameter space[31]. This difference in the domain of each algorithm leads to defining behaviors that either help or hinder the goodness of fit. The strength of `fminsearch` is that will converge rapidly to a local minimum, as long as it is near one. However, it is known to miss global minima that may produce a better fit. On the other hand, Markov chain methods like MCMC can locate minima that may be far from the initial state, but they are less likely to hone in on the exact minimum in a local sink.

In order to address the respective shortcomings of these global and local parameter fitting algorithms, we used a hybrid approach that incorporates both Nelder-Mead simplex direct search and Markov chain fitting with simulated annealing. We start with one round of `fminsearch` fitting. The resulting parameters are then passed as initial conditions to the MCMC algorithm. MCMC is iterated a sufficient number of times to yield parameters giving a good fit; in this case, 200 times. Since MCMC is effective at breaking out of local minima and finding the neighborhood of a global minimum, but less effective at actually converging to the minimum, a second round of `fminsearch` is then performed, using the results of the Markov chain fitting as initial conditions. This ensures convergence to the deepest local minimum. All parameters reported in Section

3 were determined using this sequence of fitting algorithms.

2.5. *Biologically Motivated Assumptions*

To determine the recommended parameter values for each growth function and each tumor type, we recorded the parameters of the function that best represented all trials with the same model organism at once. However, in order to determine appropriate parameter ranges, we performed fittings to each data set individually and recorded the extrema of each set of parameters. It is also assumed that *in vitro* trials are better indicators of intrinsic tumor growth rates, due to the lack of an immune system in the growth environment; and that *in vivo* trials are better indicators of animal carrying capacity, since the growth media are closer to conditions the tumor would encounter in a living organism. Thus, when relevant, intrinsic growth rates are determined from *in vitro* trials only and carrying capacities are determined from *in vivo* trials only. In cases where no carrying capacity is given, *i.e.*, the exponential and power law growth models, only *in vitro* trials are used to determine the growth rate, and the *in vitro* trials are also used to determine the exponent for the power law model.

2.6. *Fitting evaluation metrics and Parameter sensitivity analysis*

We can compare the goodness-of-fit between the output of `fminsearch` and MCMC by comparing the least-squares distances between each parameter-dependent function solution the data set to which it was fit. Using this metric, lower residuals (smaller least squares distances) suggest a better fit. We also use the least-squares residuals to calculate the Bayesian Information Criterion (BIC) for each fitting [32]. The BIC guards against over-fitting by accounting for goodness-of-fit while penalizing models that have larger numbers of parameters to be fit.

We carried out two types of parameter sensitivity analysis algorithms on the individual tumor growth models. A “local” or “one-at-a-time” parameter sensitivity analysis was performed to measure what the effect on the model outcome is when a single parameter is increased or decreased by some percentage

of its value, while keeping other parameters constant. We also carried out a Partial Rank Correlation Coefficient test (PRCC), which is intended to measure the statistical influence on the model output of parameters that have monotonic but nonlinear behavior [33, 34, 35]. Since it is impossible to determine PRCC values from a model that has only one parameter, the exponential model is excluded from PRCC analysis.

A PRCC value close to zero implies that parameters are independent of one another. If the parameter space is large, Latin Hypercube Sampling can be used to provide input to the PRCC test by random sampling from an n -dimensional space for a model with n parameter values [36, 37, 38]. These techniques are only applicable to models with more than one parameter; thus they are performed for the power law, logistic, Gompertz and von Bertalanffy models, but excluded for the exponential model.

3. Results

3.1. Tumor Growth Parameter Values

In order to determine a set of recommended parameters and appropriate ranges for each type of cancer and growth model, we fit the parameters of each growth equation to a minimum of five data sets per type of cancer. These parameters fall into three different classes: intrinsic growth rates (denoted r), exponents (denoted a) and carrying capacities (denoted K .) Two different types of fittings were performed on each set of related data sets. The *in vitro* trials for each type of cancer were fitted separately for the best fit parameters to determine an acceptable parameter range, then together with different initial conditions to determine the recommended parameter values.

We provide a catalog of suggested parameter values and ranges for ten types of cancer and five models in Table Appendix A.1. The least squares residuals and BIC values for the combined fittings can be found in Table Appendix A.2. In order to highlight the best fits and the relationship between least squares residuals and BIC values, in each row, the lowest least squares residuals values

Cancer	Model Ranking				
	1	2	3	4	5
Bladder	Power Law	Gompertz	Logistic	Exponential	Von Bertalanffy
Breast	Logistic	Gompertz	Power Law	Exponential	Von Bertalanffy
Colon	Power Law	Von Bertalanffy	Gompertz	Logistic	Exponential
HNSCC	Gompertz	Power Law	Exponential	Logistic	Von Bertalanffy
Liver	Logistic	Gompertz	Power Law	Von Bertalanffy	Exponential
Lung	Logistic	Power Law	Gompertz	Von Bertalanffy	Exponential
Melanoma	Power Law	Logistic	Exponential	Gompertz	Von Bertalanffy
Ovarian	Power Law	Exponential	Gompertz	Logistic	Von Bertalanffy
Pancreatic	Power Law	Gompertz	Logistic	Exponential	Von Bertalanffy
RCC	Power Law	Logistic	Exponential	Gompertz	Von Bertalanffy

Table 1: Model Fit Ranking According to Least Squares Residuals

are outlined with solid borders, and BIC values are outlined with dashed borders. Graphs for each individual fitting and combined fittings, as well as the residuals, parameters and sources for all fittings, can also be found in Appendix A through Appendix C. We were also able to determine a ranking of model fit for each cancer type from the evaluation metrics, shown in Table 1. This ranking was determined by comparing the sum of the least squares residuals for all individual and combined trials for each type of cancer.

3.2. Parameter Sensitivity Analysis

The “one-at-a-time” parameter sensitivity analysis was carried out by altering each parameter by 10%, with an initial condition of 1×10^4 tumor cells, running the model for 10 days, and starting with the parameters from the individually determined *in vitro* colon trials. The results are presented in Figure 1 and Figure 2 (where Figure 2 has the power law exponent removed to increase readability of the percent changes associated with the other parameters.) We

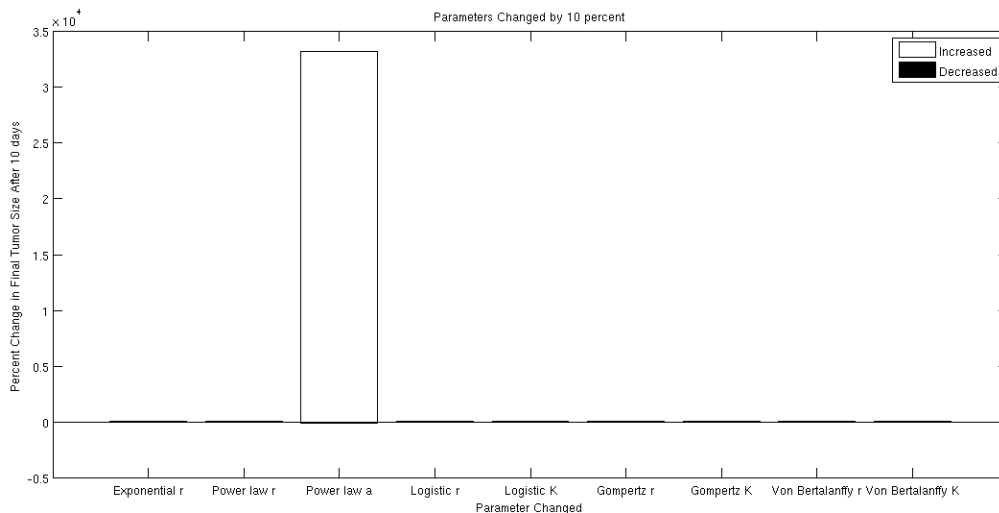


Figure 1: Local Parameter Sensitivity Analysis for Five Models, Altering Parameters by 10%

also provide a PRCC analysis over 1000 randomized parameter values using Latin hypercube sampling, which is presented in Table 2.

4. Discussion

4.1. Model Comparison

Table 1 provides a summary of the best fit models for each type of tumor. These results suggest that of the models tested, there is no one model that best approximates all forms of tumor growth. The power law provides especially close fits to data that do not appear to approach a carrying capacity, most likely because it is more flexible in approximating exponential growth dynamics. The Gompertz and logistic models outperform either the von Bertalanffy or exponential models in each case.

In some cases, the results of the fitting algorithm may be misleading. Logistic growth fittings sometimes resulted in a carrying capacity with an order of magnitude much higher than comparable trials but with the same intrinsic

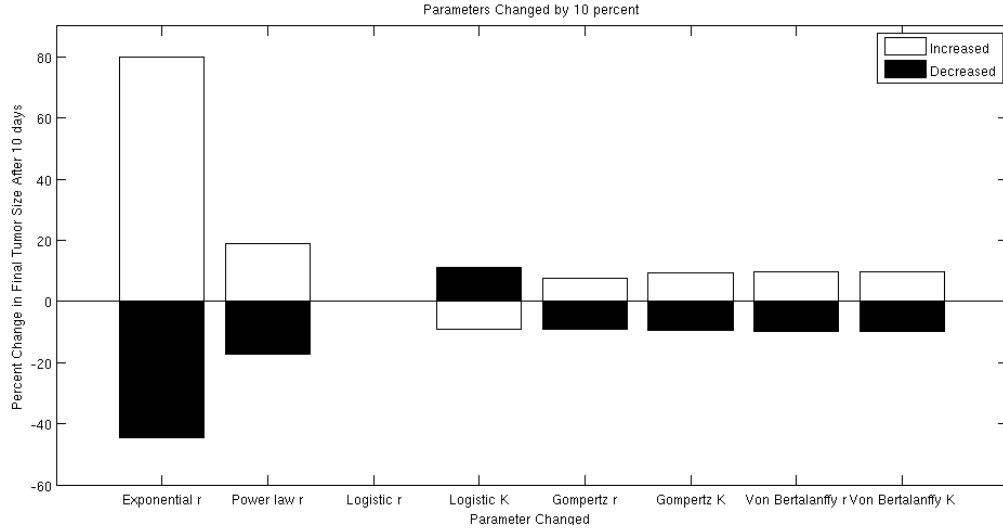


Figure 2: Local Parameter Sensitivity Analysis for Five Models, Altering Parameters by 10% (with power law a results removed)

Parameter	PRCC
Power law r	0.0412
Power law a	0
Logistic r	0
Logistic K	0
Gompertz K	0.0292
Gompertz K	0
Von Bertalanffy K	- 0.0104
Von Bertalanffy K	0

Table 2: Results of Partial Rank Correlation Coefficient Test for Two-Parameter Growth Models

growth rate as the exponential fit to the same data. This occurs with *in vivo* trial 3 for breast cancer; *in vivo* trial 4 for head and neck squamous cell carcinoma; *in vitro* trials 1, 2, and 10 and *in vivo* trial 1 and the combined *in vivo* fit for lung cancer; and *in vitro* trials 1 and 3 for ovarian cancer. When this happens, it may be that the exponential fit is a better match to the data than the logistic fit. In such a case, the logistic growth function may be approximating exponential growth by raising the carrying capacity to a number high enough so that it does not affect the fitting. This theory is supported by the least squares residuals; the least squares residuals from the exponential fit and the residuals from the logistic fit are the same when this situation occurs.

One concern that must be addressed is whether the best-fit parameters are biologically accurate [39]. We note that the best-fit von Bertalanffy parameters, which are expected to have intrinsic growth rates similar to all other models, consistently have intrinsic growth rates that are two or three orders of magnitude smaller. This is enough of an indication to doubt the biological accuracy of the von Bertalanffy parameters obtained by least-squares fitting. In addition, we have reason to question the biological relevance of the power law fittings for similar reasons.

4.2. Concerns about Power Law

We conclude from the parameter fitting process that it may not be justifiable to alter power law growth parameters, even within the range given by repeated fits. This is because the best fit power law parameters occasionally have uncharacteristically high intrinsic growth rates (e.g. *in vivo* breast cancer trials 1 and 2, the combined head and neck squamous cell carcinoma *in vivo* trial, *in vitro* lung trial 5) and exponents that are lower than the exponents in trials in the same cancer. These results suggest that power law fitting is highly sensitive, where the intrinsic growth rates rise unpredictably to accommodate lower exponents and vice versa. Therefore, although power law fits occasionally have lower residuals than the other growth laws, their unstable nature would prevent modelers from changing parameters even slightly within a specified range.

In addition, the sensitivity analyses can be used to provide a basis for our claim that the power law is not a viable model. Figure 1 suggests that a , the exponential component of the power law model, affects the model output at a much higher percentage than any other parameter in any other model. In fact, increasing a by only 10% caused the tumor to grow almost 35000% larger in only 10 days. This suggests that altering a individually would change the tumor growth behavior at a massive rate that has no biological justification. An alternative would be to alter a and r in conjunction, such that the relatively low least squares residuals for the fitting are preserved. However, as the PRCC results suggest, the relationship between a and r is highly nonlinear. This is not suggestive in and of itself—none of the other parameters had significant PRCC results—rather, we draw the conclusion in light of the results of the “one-at-a-time” parameter sensitivity analysis. In practice, a researcher seeking to lower the growth rate or raise the exponent of some of the less biologically sound power law fittings would have difficulty determining a relationship between a and r that allows the parameters to be altered while preserving the behavior of the original curve. This rigidity and extreme sensitivity is what makes the power law a less than ideal choice for a tumor growth model.

For these reasons, despite the low residual fits we found, we discourage the use of the power law model.

4.3. Parameter Fitting Algorithms

To see that the hybrid fitting algorithm is more effective than either the Nelder-Mead simplex direct search or Markov Chain method with simulated annealing, we note that a set of parameters is only accepted if the least squares residuals are lower than they were in the previous fitting. Since `fminsearch` is used to provide initial values for the Markov Chain method, the residuals of a Nelder-Mead simplex direct search on a given data set bound the residuals of the hybrid search from above. Due to the nondeterministic nature of the Markov Chain method, the residuals are not necessarily always greater than those of the hybrid method, but it is true that the residuals returned by a specific iteration of

the Markov Chain method will always be greater than the results of the hybrid algorithm using that specific iteration of the Markov Chain method. We have noted the inability of the Markov chain method to converge on global minima.

One may wonder whether using a hybrid fitting algorithm than is necessary when `fminsearch` may have been sufficient. One issue with `fminsearch` is the inability to converge to a better minimum once a local minimum is detected by the algorithm, and to improve the fitting would necessitate changing parameters by hand. Since this project required 20 separate parameter fitting trials each to 70 data sets, not including the 90 combined fittings, manually altering parameters was not a viable option. Thus, even one instance of `fminsearch` converging to a non-global minimum would necessitate the use of a stronger parameter fitting algorithm. This hybrid method was adopted after repeated difficulties with `fminsearch` which would have remained unfixable otherwise.

As a side note, it is possible to fit the equations with carrying capacities in two different ways: the first, defining the parameters to be estimated as r and K , and the second, defining the parameters to be estimated as r and $1/K$. Although theoretically equivalent, these two approaches can produce different outcomes depending on which fitting metric is used. For the logistic equation defined as

$$\frac{dP}{dt} = rP \left(1 - \frac{P}{K}\right), \quad (6)$$

it is possible that the fitting algorithm may be slower in converging to the best-fit K , because it is possible for the best-fit K to be several orders of magnitude higher than the initial condition. However, for the logistic equation defined as

$$\frac{dP}{dt} = rP(1 - bP) \quad (7)$$

where $b = \frac{1}{K}$, both the Nelder-Mead simplex direct search and the MCMC method occasionally produced results where the carrying capacity was negative. This is a result of the relative distance in parameter space from the negative real axis; 1×10^6 and -1×10^6 are much further apart than are 1×10^{-6} and -1×10^{-6} , for example. Therefore, fitting to equation (6) makes it more difficult

for either algorithm to reach negative values. We therefore recommend fitting logistic growth using the parameter forms of equation (6) in order to avoid the fittings from producing a biologically inaccurate carrying capacity.

4.4. Parameter Sensitivity Analysis

While it may seem odd to perform a sensitivity analysis on a series of models that each have only one or two parameters, these techniques can be interpreted to compare the justifiability of modifying parameters in each growth model. The PRCC values provide a measure of the strength of the relationship between two parameters, while the “one-at-a-time” parameter sensitivity analysis measures the effect of individual parameters on the model output. Therefore, while the “one-at-a-time” parameter sensitivity analysis can be used to estimate the effects of changing the value of a single parameter, the PRCC measure can tell us whether altering a single parameter while leaving the other constant is justifiable. If the “one-at-a-time” parameter sensitivity analysis reveals that altering a parameter by a small amount changes the output of the model by a significant amount, then researchers should be careful when modifying these parameters.

Acknowledgements

We would like to thank Harvey Mudd College for providing us with the resources to complete this publication, and Ami Radunskaya, the second reader.

References

References

- [1] L. de Pillis, A. Radunskaya, Some Promising Approaches to Tumor-Immune Modeling, *Contemporary Mathematics* 410 (2006) 89–105.
- [2] D. Hart, E. Shochat, Z. Agur, The growth law of primary breast cancer as inferred from mammography screening trials data, *British Journal of Cancer* 78 (1998) 382–387.

- [3] M. Elishmereni, Y. Kheifetz, H. Söndergaard, R. V. Overgaard, Z. Agur, An Integrated Disease/Pharmacokinetic/Pharmacodynamic Model Suggests Improved Interleukin-21 Regimens Validated Prospectively for Mouse Solid Cancers, *PLoS Computational Biology* 7 (2011).
- [4] Y. Zheng, H. Moore, A. Piryatinska, T. Solis, E. A. Sweet-Cordero, Mathematical modeling of tumor cell proliferation kinetics and label retention in a mouse model of lung cancer, *Cancer research* 73 (2013) 3525–3533.
- [5] T. L. Jackson, H. M. Byrne, A mathematical model to study the effects of drug resistance and vasculature on the response of solid tumors to chemotherapy, *Mathematical Biosciences* 164 (2000) 17–38.
- [6] L. de Pillis, T. Caldwell, E. Sarapata, H. Williams, Mathematical Modeling of Regulatory T Cell Effects on Renal Cell Carcinoma Treatment, *AIMS* 18 (2013) 915–943.
- [7] M. Robertson-Tessi, A. El-Kareh, A. Goriely, A mathematical model of tumor-autoimmune interactions, *Journal of Theoretical Biology* 294 (2012) 56–73.
- [8] S. Sanga, J. P. Sinek, H. B. Frieboes, M. Ferrari, J. P. Fruehauf, V. Cristini, Mathematical modeling of cancer progression and response to chemotherapy, *Expert Rev. Anticancer Ther.* 6 (2006) 1361–1376.
- [9] G. Lillacci, M. Khammash, Parameter estimation and model selection in computational biology, *PLoS computational biology* 6 (2010) e1000696.
- [10] M. F. Dempsey, B. R. Condon, D. M. Hadley, Measurement of tumor size in recurrent malignant glioma: 1d, 2d, or 3d?, *American journal of neuroradiology* 26 (2005) 770–776.
- [11] K. Kisfalvi, G. Eibl, J. Sinnett-Smith, Metformin Disrupts Crosstalk between G Protein—Coupled Receptor and Insulin Receptor Signaling Systems and Inhibits Pancreatic Cancer Growth, *Cancer Research* 69 (2009) 6539–6545.

- [12] J. L. Ricker, Z. Chen, X. P. Yang, 2-Methoxyestradiol Inhibits Hypoxia-Inducible Factor 1α , Tumor Growth, and Angiogenesis and Augments Paclitaxel Efficacy in Head and Neck Squamous Cell Carcinoma, *Clinical Cancer Research* 10 (2004) 8665–8673.
- [13] J. B. Sunwoo, Z. Chen, G. Dong, Novel Proteasome Inhibitor PS-341 Inhibits Activation of Nuclear Factor- κ B, Cell Survival, Tumor Growth, and Angiogenesis in Squamous Cell Carcinoma, *Clinical Cancer Research* 7 (2001) 1419–1428.
- [14] H. Boukerche, O. Berthier-Vergnes, M. Bailly, J. Dore, L. Leung, J. McGregor, A monoclonal antibody (LYP18) directed against the blood platelet glycoprotein IIb/IIIa complex inhibits human melanoma growth in vivo, *Blood* 74 (1989) 909–912.
- [15] H. Juhl, S. G. Downing, A. Wellstein, F. Czubayko, HER-2/neu Is Rate-limiting for Ovarian Cancer Growth, *Journal of Biological Chemistry* 272 (1997) 29482–29486.
- [16] A. J. Murgo, Inhibition of B16-BL6 Melanoma Growth in Mice by Methionine-Enkephalin, *Journal of the National Cancer Institute* 75 (1985) 476–482.
- [17] Y. D. Burke, M. J. Stark, S. L. Roach, S. E. Sen, P. L. Crowell, Inhibition of Pancreatic Cancer Growth by the Dietary Isoprenoids Farnesol and Geraniol, *Lipids* 32 (1997) 151–156.
- [18] N. Fujimoto, A. Sugita, Y. Terasawa, M. Kato, Observations on the Growth Rate of Renal Cell Carcinoma, *International Journal of Urology* 2 (1995) 71–76.
- [19] T. Okegawa, R.-C. Pong, Y. Li, The Mechanism of the Growth-inhibitory Effect of Coxsackie and Adenovirus Receptor (CAR) on Human Bladder Cancer: A Functional Analysis of CAR Protein Structure, *Cancer Research* 61 (2001) 6592–6600.

- [20] T. Fujiwara, E. A. Grimm, T. Mukhopadhyay, A Retroviral Wild-type p53 Expression Vector Penetrates Human Lung Cancer Spheroids and Inhibits Growth by Inducing Apoptosis, *Cancer Research* 53 (1993) 4129–4133.
- [21] M. H. Ahonen, Y.-H. Zhuang, R. Aine, T. Ylikomi, P. Tuohimaa, Androgen receptor and vitamin D receptor in human ovarian cancer: Growth stimulation and inhibition by ligands, *International Journal of Cancer* 86 (2000) 40–46.
- [22] T. Takahashi, D. Carbone, T. Takahashi, Wild-type but not Mutant p53 Suppresses the Growth of Human Lung Cancer Cells Bearing Multiple Genetic Lesions, *Cancer Research* 52 (1992) 2340–2343.
- [23] A. Richmond, D. H. Lawson, D. W. Nixon, Extraction of a Melanoma Growth-stimulatory Activity from Culture Medium Conditioned by the Hs0294 Human Melanoma Cell Line, *Cancer Research* 43 (1983) 2106–2112.
- [24] N. Reinmuth, F. Fan, W. Liu, A. A. Parikh, O. Stoeltzing, Y. D. Jung, C. D. Bucana, R. Radinsky, G. E. Gallick, L. M. Ellis, Impact of Insulin-Like Growth Factor Receptor-I Function on Angiogenesis, Growth, and Metastasis of Colon Cancer, *Laboratory Investigation* 82 (2002) 1377–1389.
- [25] H. Nakata, Y. Kikuchi, T. Tode, J. Hirata, T. Kita, K. Ishii, K. Kudoh, I. Nagata, N. Shinomiya, Inhibitory Effects of Ginsenoside Rh₂ on Tumor Growth in Nude Mice Bearing Human Ovarian Cancer Cells, *Japanese Journal of Cancer Research* 89 (1998) 733–740.
- [26] S. Caltagirone, C. Rossi, A. Poggi, F. O. Ranelletti, P. G. Natali, M. Brunetti, F. B. Aiello, M. Piantelli, Flavonoids apigenin and quercetin inhibit melanoma growth and metastatic potential, *International Journal of Cancer* 87 (2000) 595–600.
- [27] J. C. Lagarias, J. A. Reed, M. H. Wright, P. E. Wright, Convergence

- Properties of the Nelder-Mead Simplex Method in Low Dimensions, *SIAM Journal on Optimization* 9 (1998) 112–147.
- [28] G. Winkler, *Image Analysis, Random Fields and Markov Chain Monte Carlo Methods*, 2 ed., Springer-Verlag Berlin Heidelberg New York, 2003.
- [29] W. W. R. Gilks, S. Richardson, D. J. Spiegelhalter, *Markov Chain Monte Carlo in Practice: Interdisciplinary Statistics*, 1 ed., Chapman & Hall/CRC, 1996.
- [30] S. Brooks, A. Gelman, G. L. Jones, X.-L. Meng, *Handbook of Markov Chain Monte Carlo*, 1 ed., Chapman & Hall/CRC, 2011.
- [31] M. Ashyraliyev, Y. Fomekong-Nanfack, J. A. Kaandorp, J. G. Joke G. Blom, *Systems biology: parameter estimation for biochemical models*, *FEBS Journal* 276 (2009) 886–902.
- [32] A. O’Hagan, J. Forster, M. G. Kendall, *Bayesian inference*, Arnold London, 2004.
- [33] B. Gomero, *Latin Hypercube Sampling and Partial Rank Correlation Coefficient Analysis Applied to an Optimal Control Problem*, Master’s Thesis, University of Tennessee (2012).
- [34] R. L. Iman, J. C. Helton, *The repeatability of uncertainty and sensitivity analyses for complex probabilistic risk assessments*, *Risk Analysis* 11 (1991) 591–606.
- [35] D. Hamby, *A review of techniques for parameter sensitivity analysis of environmental models*, *Environmental Monitoring and Assessment* 32 (1994) 135–154.
- [36] S. Blower, H. Dowlatabadi, *Sensitivity and uncertainty analysis of complex models of disease transmission: an HIV model, as an example*, *International Statistical Review/Revue Internationale de Statistique* (1994) 229–243.

- [37] R. L. Iman, J. C. Helton, An investigation of uncertainty and sensitivity analysis techniques for computer models, *Risk analysis* 8 (1988) 71–90.
- [38] R. L. Iman, W. Conover, Small sample sensitivity analysis techniques for computer models. with an application to risk assessment, *Communications in statistics-theory and methods* 9 (1980) 1749–1842.
- [39] D. F. Slezak, C. Surez, G. A. Cecchi, G. Marshall, G. Stolovitzky, When the Optimal Is Not the Best: Parameter Estimation in Complex Biological Models, *PLoS* 5 (2010).
- [40] R. Golshani, L. Lopez, V. Estrella, Hyaluronic Acid Synthase-1 Expression Regulates Bladder Cancer Growth, Invasion, and Angiogenesis through CD44, *Cancer Research* 68 (2008) 483–491.
- [41] M. Kamada, A. So, M. Muramaki, Hsp27 knockdown using nucleotide-based therapies inhibit tumor growth and enhance chemotherapy in human bladder cancer cells, *Molecular Cancer Therapeutics* 6 (2007) 299–308.
- [42] H. Miyake, I. Hara, S. Kamidono, Synergistic Chemosensitization and Inhibition of Tumor Growth and Metastasis by the Antisense Oligodeoxynucleotide Targeting Clusterin Gene in a Human Bladder Cancer Model, *Clinical Cancer Research* 7 (2001) 4245–4252.
- [43] S. Ohnishi, S. Ohnami, F. Laub, K. Aoki, K. Suzuki, Y. Kanai, K. Haga, M. Asaka, F. Ramirez, T. Yoshida, Downregulation and growth inhibitory effect of epithelial-type Krüppel-like transcription factor KLF4, but not KLF5, in bladder cancer, *Biochemical and Biophysical Research Communications* 308 (2003) 251–256.
- [44] Z. Du, S. Hou, The Anti-Angiogenic Activity of Human Endostatin Inhibits Bladder Cancer Growth and Its Mechanism, *The Journal of Urology* 170 (2003) 2000–2003.
- [45] P. J. P. Coopman, M. T. H. Do, M. Barth, E. T. Bowden, A. J. Hayes, E. Basyuk, J. K. Blancatok, P. R. Vezza, S. W. McLeskey, P. H. Mangeat,

- S. C. Mueller, The Syk tyrosine kinase suppresses malignant growth of human breast cancer cells, *Nature* 406 (2000) 742–747.
- [46] R. Lu, G. Serrero, Resveratrol, a Natural Product Derived From Grape, Exhibits Antiestrogenic Activity and Inhibits the Growth of Human Breast Cancer Cells, *Journal of Cellular Physiology* 179 (1999) 297–304.
- [47] H. Nakagawa, K. Tsuta, K. Kiuchi, H. Senzaki, K. Tanaka, K. Hioki, A. Tsubura, Growth inhibitory effects of diallyl disulde on human breast cancer cell lines, *Carcinogenesis* 22 (2001) 891–897.
- [48] M. C. P. Smith, K. E. Luker, J. R. Garbow, CXCR4 Regulates Growth of Both Primary and Metastatic Breast Cancer, *Cancer Research* 64 (2004) 8604–8612.
- [49] P. Sarraf, E. Mueller, D. Jones, F. J. King, D. J. DeAngelo, J. B. Partridge, S. A. Holden, L. B. Chen, S. Singer, C. Fletcher, B. M. Spiegelman, Differentiation and reversal of malignant changes in colon cancer through PPAR γ , *Nature Medicine* 4 (1998) 1046–1052.
- [50] H. Sheng, J. Shao, S. C. Kirkland, P. Isakson, R. J. Coffey, J. Morrow, R. D. Beauchamp, R. N. DuBois, Inhibition of Human Colon Cancer Cell Growth by Selective Inhibition of Cyclooxygenase-2, *The Journal of Clinical Investigation* 99 (1997) 2254–2259.
- [51] R. S. Warren, H. Yuan, M. R. Matli, N. A. Gillett, N. Ferrara, Regulation by Vascular Endothelial Growth Factor of Human Colon Cancer Tumorigenesis in a Mouse Model of Experimental Liver Metastasis, *Journal of Clinical Investigation* 95 (1995) 1789–1797.
- [52] M. Todaro, M. P. Alea, A. B. Di Stefano, P. Cammareri, L. Vermeulen, F. Iovino, C. Tripodo, A. Russo, G. Gulotta, J. P. Medema, G. Stassi, Colon Cancer Stem Cells Dictate Tumor Growth and Resist Cell Death by Production of Interleukin-4, *Cell Stem Cell* 1 (2007) 389–402.

- [53] D. C. Duffey, Z. Chen, G. Dong, Expression of a Dominant-Negative Mutant Inhibitor- κ B α of Nuclear Factor- κ B in Human Head and Neck Squamous Cell Carcinoma Inhibits Survival, Proinflammatory Cytokine Expression, and Tumor Growth in Vivo, *Cancer Research* 59 (1999) 3468–3474.
- [54] T.-J. Liu, M. Wang, R. L. Breau, Y. Henderson, A. K. El-Naggar, K. D. Steck, M. W. Sicard, G. L. Clayman, Apoptosis induction by E2F-1 via adenoviral-mediated gene transfer results in growth suppression of head and neck squamous cell carcinoma cell lines, *Cancer Gene Therapy* 6 (1999) 163–172.
- [55] M. M. LoTempio, M. S. Veena, H. L. Steele, Curcumin Suppresses Growth of Head and Neck Squamous Cell Carcinoma, *Clinical Cancer Research* 11 (2005) 6994–7002.
- [56] H. Huynh, P. K. Chow, N. Palanisamy, M. Salto-Tellez, Bevacizumab and rapamycin induce growth suppression in mouse models of hepatocellular carcinoma, *Journal of Hepatology* 49 (2008) 52–60.
- [57] C.-R. Jung, J. Yoo, Y. J. Jang, S. Kim, I.-S. Chu, Y. I. Yeom, J. Y. Choi, D.-S. Im, Adenovirus-Mediated Transfer of siRNA Against PTTG1 Inhibits Liver Cancer Cell Growth In Vitro and In Vivo, *Journal of Hepatology* 43 (2006) 1042–1052.
- [58] Y. Liu, R. T. Poon, Q. Li, Both Antiangiogenesis- and Angiogenesis-Independent Effects Are Responsible for Hepatocellular Carcinoma Growth Arrest by Tyrosine Kinase Inhibitor PTK787/ZK222584, *Cancer Research* 65 (2005) 3691–3699.
- [59] C.-M. Wong, J. W.-P. Yam, Y.-P. Ching, Rho GTPase-Activating Protein Deleted in Liver Cancer Suppresses Cell Proliferation and Invasion in Hepatocellular Carcinoma, *Cancer Research* 65 (2005) 8861–8868.
- [60] L. Zender, W. Xue, J. Zuber, C. P. Semighini, A. Krasnitz, B. Ma, P. Zender, S. Kubicka, J. M. Luk, P. Schirmacher, W. R. McCombie, M. Wigler,

- J. Hicks, G. J. Hannon, S. Powers, S. W. Lowe, An Oncogenomics-Based In Vivo RNAi Screen Identifies Tumor Suppressors in Liver Cancer, *Cell* 135 (2008) 852–864.
- [61] A. Esquela-Kerscher, P. Trang, J. F. Wiggins, L. Patrawala, A. Cheng, L. Ford, J. B. Weidhaas, D. Brown, A. G. Bader, F. J. Slack, The let-7 microRNA reduces tumor growth in mouse models of lung cancer, *Cell Cycle* 7 (2008) 759–764.
- [62] M. Fabbri, D. Iliopoulos, F. Trapasso, R. I. Aqeilan, A. Cimmino, N. Zanasi, S. Yendamuri, S.-Y. Han, D. Amadori, K. Huebner, C. M. Croce, WWOX gene restoration prevents lung cancer growth in vitro and in vivo, *PNAS* 102 (2005) 15611–15616.
- [63] Y. Tsubouchi, H. Sano, Y. Kawahito, S. Mukai, R. Yamada, M. Kohno, K.-i. Inoue, T. Hla, M. Kondo, Inhibition of Human Lung Cancer Cell Growth by the Peroxisome Proliferator-Activated Receptor- γ Agonists through Induction of Apoptosis, *Biochemical and Biophysical Research Communications* 270 (2000) 400–405.
- [64] T. W. Moody, F. Zia, M. Draoui, D. E. Brenneman, M. Fridkin, A. Davidson, I. Gozes, A vasoactive intestinal peptide antagonist inhibits non-small cell lung cancer growth, *Biochemistry* 90 (1993) 4345–4349.
- [65] S. Sharma, M. Stolina, Y. Lin, B. Gardner, P. W. Miller, M. Kronenberg, S. M. Dubinett, T Cell-Derived IL-10 Promotes Lung Cancer Growth by Suppressing Both T Cell and APC Function, *Journal of Immunology* 163 (1999) 5020–5028.
- [66] M. D. Bregman, C. Funk, M. Fukushima, Inhibition of Human Melanoma Growth by Prostaglandin A, D, and J Analogues, *Cancer Research* 46 (1986) 2740–2744.
- [67] R. Kunstfeld, G. Wickenhauser, U. Michaelis, M. Teifel, W. Umek, K. Naujoks, K. Wolsh, P. Petzelbauer, Paclitaxel Encapsulated in Cationic Lipo-

- somes Diminishes Tumor Angiogenesis and Melanoma Growth in a Humanized SCID Mouse Model, *Journal of Investigative Dermatology* 120 (2003) 476–482.
- [68] E. Petitclerc, S. Strömblad, T. L. von Schalscha, Integrin $\alpha_V\beta_3$ Promotes M21 Melanoma Growth in Human Skin by Regulating Tumor Cell Survival, *Cancer Research* 59 (1999) 2724–2730.
- [69] R. Abe, T. Shimizu, H. Sugawara, H. Watanabe, H. Nakamura, H. Choei, N. Sasaki, S.-i. Yamagishi, M. Takeuchi, H. Shimizu, Regulation of Human Melanoma Growth and Metastasis by AGE-AGE Receptor Interactions, *Journal of Investigative Dermatology* 122 (2004) 461–467.
- [70] F. Polato, A. Codegani, R. Fruscio, PRL-3 Phosphatase Is Implicated in Ovarian Cancer Growth, *Clinical Cancer Research* 11 (2005) 6835–6839.
- [71] Y. Yokoyama, M. Dhanabal, A. W. Griffioen, Synergy between Angiostatin and Endostatin: Inhibition of Ovarian Cancer Growth, *Cancer Research* 60 (2000) 2190–2196.
- [72] T. Ito, S. Kawata, S. Tamura, T. Igura, T. Nagase, J.-i. Miyagawa, E. Yamazaki, H. Ishiguro, Y. Matsuzawa, Suppression of Human Pancreatic Cancer Growth in BALB/c Nude Mice by Manumycin, a Farnesyl: Protein Transferase Inhibitor, *Cancer Science* 87 (1996) 113–116.
- [73] M. Vogler, H. Walczak, D. Stadel, Targeting XIAP Bypasses Bcl-2 Mediated Resistance to TRAIL and Cooperates with TRAIL to Suppress Pancreatic Cancer Growth In vitro and In vivo, *Cancer Research* 68 (2009) 7956–7965.
- [74] E. E. Zervos, J. G. Norman, W. R. Gower, M. G. Franz, A. S. Rosemurgy, Matrix Metalloproteinase Inhibition Attenuates Human Pancreatic Cancer Growth in Vitro and Decreases Mortality and Tumorigenesis in Vivo, *Journal of Surgical Research* 69 (1997) 367–371.

- [75] M. Dhanabal, R. Ramchandran, R. Volk, Endostatin : Yeast Production, Mutants, and Antitumor Effect in Renal Cell Carcinoma, *Cancer Research* 59 (1999) 189–197.
- [76] B. Lieubeau-Teillet, J. Rak, S. Jothy, von Hippel-Lindau Gene-mediated Growth Suppression and Induction of Differentiation in Renal Cell Carcinoma Cells Grown as Multicellular Tumor Spheroids, *Cancer Research* 58 (1998) 4957–4962.
- [77] D. Huang, Y. Ding, W.-M. Luo, Inhibition of MAPK Kinase Signaling Pathways Suppressed Renal Cell Carcinoma Growth and Angiogenesis In vivo, *Cancer Research* 68 (2008) 81–88.
- [78] K.-i. Inoue, Y. Kawahito, Y. Tsubouchi, M. Kohno, R. Yoshimura, T. Yoshikawa, H. Sano, Expression of Peroxisome Proliferator-Activated Receptor γ in Renal Cell Carcinoma and Growth Inhibition by Its Agonists, *Biochemical and Biophysical Research Communications* 287 (2001) 727–732.
- [79] M. Schirner, J. Hoffmann, A. Menrad, Antiangiogenic chemotherapeutic agents: characterization in comparison to their tumor growth inhibition in human renal cell carcinoma models., *Clinical Cancer Research* 4 (1998) 1331–1336.
- [80] W. Shi, D. Siemann, Inhibition of renal cell carcinoma angiogenesis and growth by antisense oligonucleotides targeting vascular endothelial growth factor, *British Journal of Cancer* 87 (2002) 119–126.
- [81] M. Prewett, M. Rothman, H. Waksal, Mouse-human chimeric anti-epidermal growth factor receptor antibody C225 inhibits the growth of human renal cell carcinoma xenografts in nude mice., *Clinical Cancer Research* 4 (1998) 2957–2966.

Appendix A. Supplemental Materials: Tumor Growth Parameters

We present a catalog of suggested parameter values and ranges for ten types of cancer and the five canonical growth functions that were considered. The parameters found using a hybrid fitting algorithm to a minimum of five data sets per type of tumor are given in Table Appendix A.1. For comparison purposes, the least squares residuals and BIC values are presented in Table Appendix A.2. We highlight the lowest least squares residuals in each row with a solid border and the lowest BIC values in each row with a dashed border.

Cancer	Exponential	Power Law	Logistic	Gompertz	Von Bertalanffy	
Bladder	r	0.0165:(0.0942):0.1919	0.0033:(5.5976):51.2297	0.1378:(1.3454):9.0473	0.0075:(0.2893):0.2893	3.6E-4:(0.0392):0.0037
	a, K	0.6839:(0.8582):1.1552	0.6839:(0.8582):1.1552	5.36E4:(1.24E9):1.91E10	3.07E5:(8.10E6):9.01E11	1.5E4:(1.5E4):1.11E11
Breast	r	0.183:(0.4593):1.3311	0.0456:(5.3077):3988.3	0.183:(1.4808):1.5488	0.0095:(0.4834):0.4834	6.17E-5:(2.95E-4):0.0062
	a, K	0.3151:(0.8299):1.122	0.3151:(0.8299):1.122	9.45E5:(2.46E9):2.73E9	1.92E6:(1.53E10):4.24E13	3.95E8:(1.06E10):5.2E11
Colon	r	0.4555:(0.4816):0.5533	1.606:(1.606):35.339	0.5521:(0.5775):0.8401	0.0608:(0.0608):0.2405	1.8E-4:(1.8E-4):2.6E4
	a, K	0.5521:(0.8819):0.8819	0.5521:(0.8819):0.8819	2.32E8:(8.02E8):3.65E51.47E9	3.78E8:(9.90E8):1.44E12	1.65E9:(4.49E10):2.04E11
HNSCC	r	0.0277:(0.0286):0.5014	0.0728:(0.6353):42.0098	0.0309:(0.0328):0.576	0.0017:(0.0044):0.1218	1.19E-5:(1.19E-5):1.51E-4
	a, K	0.1749:(0.1754):0.5307	0.7384:(0.8376):0.9597	5.17E6:(1.37E7):1.37E7	1.11E7:(1.17E12):7.01E14	7.66E8:(2.94E10):2.94E10
Liver	r	0.1749:(0.1754):0.5307	:2.8332(278.3617):738.1756	0.2402:(0.2421):0.5982	0.0637:(0.0670):0.0730	6.99E-5:(6.99E-5):2.53E-4
	a, K	0.5685:(0.619):0.8589	0.5685:(0.619):0.8589	1.34E6:(4.85E8):2.44E9	3.04E8:(4.96E8):1.60E13	2.51E7:(5.01E8):3.55E10
Lung	r	0.0804:(0.3358):0.6501	0.0026:(0.2814):2.15E6	0.35:(0.381):1.3577	0.004:(0.0049):0.658	2.93E-5:(2.93E-5):0.1143
	a, K	0.0908:(0.1502):0.2414	-0.0806:(0.995):1.3872	3.77E7:(1.36E12):1.36E12	3.85E7:(2.84E21):2.84E21	4.02E7:(9.70E11):2.07E12
Melanoma	r	0.0908:(0.1502):0.2414	0.0081:(0.0081):299.271	0.1061:(0.1502):0.4766	0.0043:(0.0043):0.2872	0.0015:(0.5303):0.5303
	a, K	0.5442:(1.1596):1.1596	0.5442:(1.1596):1.1596	4.87E7:(7.36E8):2.36E9	7.93E7:(5.02E8):3.48E9	9.48E7:(4.06E8):3.49E11
Ovarian	r	0.5087:(0.6765):0.7634	1.42E-4:(2.3356):3.58E7	0.5087:(0.823):2.4545	0.0193:(0.0815):1.4489	3.35E-4:(4.96E-4):0.7245
	a, K	0.0541:(0.3093):0.4122	-0.4252:(0.8963):1.7012	8.08E8:(3.07E12):3.07E12	2.06E9:(9.41E19):9.41E19	9.32E10:(1.20E13):1.20E13
Pancreatic	r	0.0541:(0.3093):0.4122	2.84E-5:(0.668):13.216	0.0541:(0.348):0.4645	0.0023:(0.0524):0.1566	1.92E-5:(0.0055):0.0055
	a, K	0.3674:(0.4504):0.5568	0.7126:(0.9102):1.493	5.69E7:(5.69E7):7.62E8	7.09E7:(7.09E7):5.81E15	1.79E9:(6.28E9):2.81E11
RCC	r	0.3674:(0.4504):0.5568	0.6554:(44.7253):172.3193	0.3884:(0.5719):1.365	0.0342:(0.0773):0.8647	3.5E-6:(3.5E-6):0.4437
	a, K	0.2805:(0.6182):0.9473	0.2805:(0.6182):0.9473	2.49E8:(8.91E8):1.41E9	3.02E8:(3.02E8):4.19E11	2.95E8:(2.95E8):1.46E11

Table Appendix A.1: Recommended Parameter Values and Ranges for Ten Different Types of Cancer and Five ODE Growth

Laws

Trial	Exponential		Power Law		Logistic		Gompertz		Von Bertalanffy	
	Residuals	BIC	Residuals	BIC	Residuals	BIC	Residuals	BIC	Residuals	BIC
Bladder <i>in vitro</i>	7.43E10	97.117	4.22E10	96.241	3.00E10	94.876	3.30E8	[76.837]	2.40E11	103.194
Bladder <i>in vivo</i>	7.43E10	2363.3	4.22E10	2339.9	3.00E10	2353.2	2.21E17	[2329.9]	1.09E18	2337.0
Breast <i>in vitro</i>	5.70E12	506.07	2.04E12	[489.52]	2.28E12	491.59	2.08E12	489.87	2.39E12	492.55
Breast <i>in vivo</i>	2.10E18	749.61	1.40E18	744.80	6.02E17	[728.80]	1.01E18	738.68	8.92E18	780.03
Colon <i>in vitro</i>	1.72E9	228.87	1.18E9	226.87	1.18E9	226.88	1.18E9	[226.83]	1.03E10	252.80
Colon <i>in vivo</i>	1.79E18	1799.3	8.71E17	1769.3	1.33E18	1789.1	1.12E18	1781.1	8.60E17	[1768.6]
HNSCC <i>in vitro</i>	6.02E17	1531.0	5.00E17	[1527.0]	5.57E17	1532.4	5.09E17	1527.8	1.17E18	1562.1
HNSCC <i>in vivo</i>	5.03E13	519.78	3.07E13	[513.78]	3.77E13	517.48	5.13E13	523.02	2.30E14	550.03
Liver <i>in vitro</i>	1.51E17	770.77	2.15E16	732.92	9.64E15	[716.08]	1.59E16	726.60	3.60E17	792.09
Liver <i>in vivo</i>	1.17E19	1809.5	8.60E18	1799.3	7.51E18	[1793.2]	7.56E18	1793.4	7.83E18	1795.0
Lung <i>in vitro</i>	1.75E22	4201.0	1.74E22	4214.2	1.29E22	[4187.3]	2.14E22	4232.6	1.75E22	4214.6
Lung <i>in vivo</i>	1.86E18	[861.64]	1.64E18	861.85	1.86E18	864.73	1.90E18	865.11	2.86E18	874.11
Melanoma <i>in vitro</i>	5.25E18	688.49	1.26E18	[667.04]	5.25E18	691.32	5.67E18	692.62	7.99E18	698.45
Melanoma <i>in vivo</i>	7.20E18	1903.2	2.42E18	[1854.8]	6.48E18	1902.0	7.67E18	1910.1	8.34E18	1914.2
Ovarian <i>in vitro</i>	1.60E11	[372.25]	1.58E11	374.82	1.56E11	374.55	1.58E11	374.80	2.20E11	380.09
Ovarian <i>in vivo</i>	3.27E18	[758.01]	2.88E18	758.54	3.27E18	760.95	7.45E18	788.85	3.44E20	849.44
Pancreatic <i>in vitro</i>	5.87E5	[61.088]	5.86E5	62.534	5.48E5	62.359	5.79E5	62.630	2.09E6	69.045
Pancreatic <i>in vivo</i>	5.79E16	1401.1	3.83E16	[1388.2]	4.50E16	1394.7	4.15E16	1391.4	3.83E16	[1388.2]
RCC <i>in vitro</i>	6.90E11	1140.5	6.40E11	1138.9	4.71E11	1131.3	4.92E11	[668.17]	1.12E12	691.14
RCC <i>in vivo</i>	1.59E18	[2052.6]	1.51E18	2054.0	1.59E18	2056.6	1.80E18	2063.5	1.83E18	2064.4

Table Appendix A.2: Model Evaluation Metrics for Combined Experimental Data Fittings

Appendix B. Supplemental Materials: Sources of Data for Parameter Values

A large number of individual studies were gathered in determining appropriate timescale tumor growth data sets to be used in the fitting process. Not only are the sources for each type of cancer listed, the individual cell lines used in each paper are included for posterity. Some papers, which used tissue samples from human subjects as the source of cancerous cells, did not specify a cell line.

Cancer and Cell Line	Sources
Bladder Cancer	
HT1376	[40]
UMUC-3	[41]
KoTCC-1	[42]
EJ-1	[43, 44]
Breast Cancer	
MDA-MB-435BAG	[45]
MCF-7	[46]
KPL-1	[47]
4T1-GFP-FL	[48]
Colon Cancer	
KM12L4	[24]
Moser	[49]
HCT116	[49, 50]
CX-1	[49]
HCA7	[50]
LS LiM6	[51]
Unspecified	[52]
Head and Neck Squamous Cell Carcinoma	
UM-SCC-9	[53]
Tu-138	[54]

Table Appendix B.1: Sources of Timescale Data by Type of Cancer and Cell

Cancer and Cell Line	Sources
Tu-167	[54]
686LN	[54]
CAL27	[55]
UM-SCC-X	[12]
PAM-LY2	[13]
Hepatocellular Carcinoma	
HCC-26-1004	[56]
HCC-2-1318	[56]
SH-J1	[57]
PLC	[58]
Hep3B	[58]
SMMC-7721	[59]
Unspecified	[60]
Lung Cancer	
SW-900	[61]
H226	[61]
A549	[61]
	[62]
	[63]
H460	[62]
H1299	[62]
U2020	[62]
H322a	[20]
WT226b	[20]
NCI-H727	[64]
3LL	[65]
NCI-H358	[22]
H841	[63]

Table Appendix B.1: Sources of Timescale Data by Type of Cancer and Cell Line

Cancer and Cell Line	Sources
pc14	[63]
Melanoma	
M3Dau	[14]
MIRW5	[66]
B16-BL6	[26, 16]
A-375	[67]
M21	[68]
Hs0294	[23]
Unspecified	[69]
Ovarian Cancer	
SKOV-3	[15, 70]
HRA	[25]
A2780	[70]
IGROV-1	[70]
HCT-116	[70]
MA148	[71]
Pancreatic Cancer	
PC-1	[17]
MIAPaCa-2	[72, 11]
PANC-1	[11]
PancTu1	[73]
HPAC	[74]
Renal Cell Carcinoma	
786-O	[75, 76]
ACHN	[77]
A-498	[77]
Caki-1	[78, 79]
	[80]

Table Appendix B.1: Sources of Timescale Data by Type of Cancer and Cell Line

Cancer and Cell Line	Sources
SK-RC-29	[81]
Caki-2	[79]
Unspecified	[18]

Table Appendix B.1: Sources of Timescale Data by Type of Cancer and Cell Line

Appendix C. Supplemental Materials: Results of Parameter Fittings

Individual data sets are labeled with the year and author, and given a unique identifier: either the label they were presented with in the figure from which the data originated, or the cell line that is used in the paper.

In some cases, the line representing the result of the parameter fitting is not visible. This happens for one of two reasons: a large difference between orders of magnitude in separate data sets, limiting the available space for data sets with smaller orders of magnitude; or because two or more data sets started with the same initial condition, causing the combined fitting result to produce the same curve. A complete list of all of the parameter fittings that are not visible, and the reason for why they cannot be seen, is given below:

- In the combined *in vitro* bladder cancer trials, the AS clusterin and MM control trials of Miyake 2001 share an initial condition, hence only the MM control fitting is visible.
- In the combined *in vitro* breast cancer trials, the three Smith 2004 trials share the same initial condition, so the purple curve indicates the fitting to all three of these trials.
- In the combined *in vivo* breast cancer trials, the two Coopman 2000 trials share an initial condition, thus the green curve represents the fitting to both trials.

- In the combined *in vitro* colon cancer trials, the Moser and HCT116 trials have the same initial condition, so the green curve represents the combined fitting to both.
- In the combined *in vivo* colon cancer trials, two sets of trials have the same initial condition—the two Reinmuth 2002 trials and the two Warren 1995 trials. As a result, the orange curves account for both Reinmuth 2002 trials and the pink curves to both Warren 1995 trials.
- In the combined *in vivo* head and neck squamous cell carcinoma trials, the three Liu 1999 trials start with the same initial conditions, hence the teal curve represents the combined fitting to all three data sets.
- In the combined *in vitro* hepatocellular carcinoma trials, the Huynh 2008 trials share an initial condition, so the green curve represents the fitting to both data sets.
- In the combined *in vivo* hepatocellular carcinoma trials, the Liu 2005 data sets have the same initial condition, so the teal curve indicates the fitting to both data sets.
- In the individual *in vitro* lung cancer trials, Fig. 4D from Fabbri 2005 was cropped from the graph because it was two orders of magnitude higher than the next largest tumor, making the other 12 trials impossible to distinguish. Despite its exclusion here, it was used in the fitting analysis.
- In the combined *in vitro* lung cancer trials, not only is Fig. 4D from Fabbri 2005 excluded, but several trials from the same study have the same initial conditions (*i.e.*, the four visible Fabbri 2005 trials, SW-900 and A549 from Esquela-Kerscher, and all three Fujiwara trials.) For this figure, the seafoam green curve is the fit for all 4 visible Fabbri 2005 trials, the SW-900 and A549 trials from Esquela-Kerscher are both represented by the yellow curve, and all three Fujiwara trials are represented by the purple curve. Additionally, for the von Bertalanffy fitting, the data sets from

Fujiwara 1993 and Takahashi 1992 are hidden by Fig. 3 from Tsubouchi 2000, presumably because their initial conditions are sufficiently close to each other.

- In the *in vivo* melanoma trials, the Boucherke 1989 trial is difficult to see because of its relatively low order of magnitude, but is visible along the bottom of the graphs.
- In the combined *in vitro* ovarian cancer trials, the A2780 and SKOV-3 trials have the same initial condition, and the IGROV-1 and HCT-116 trials have the same initial condition. As a result, the green curve represents the fitting to the first two trials, and the purple curve is the fitting to the last two trials.

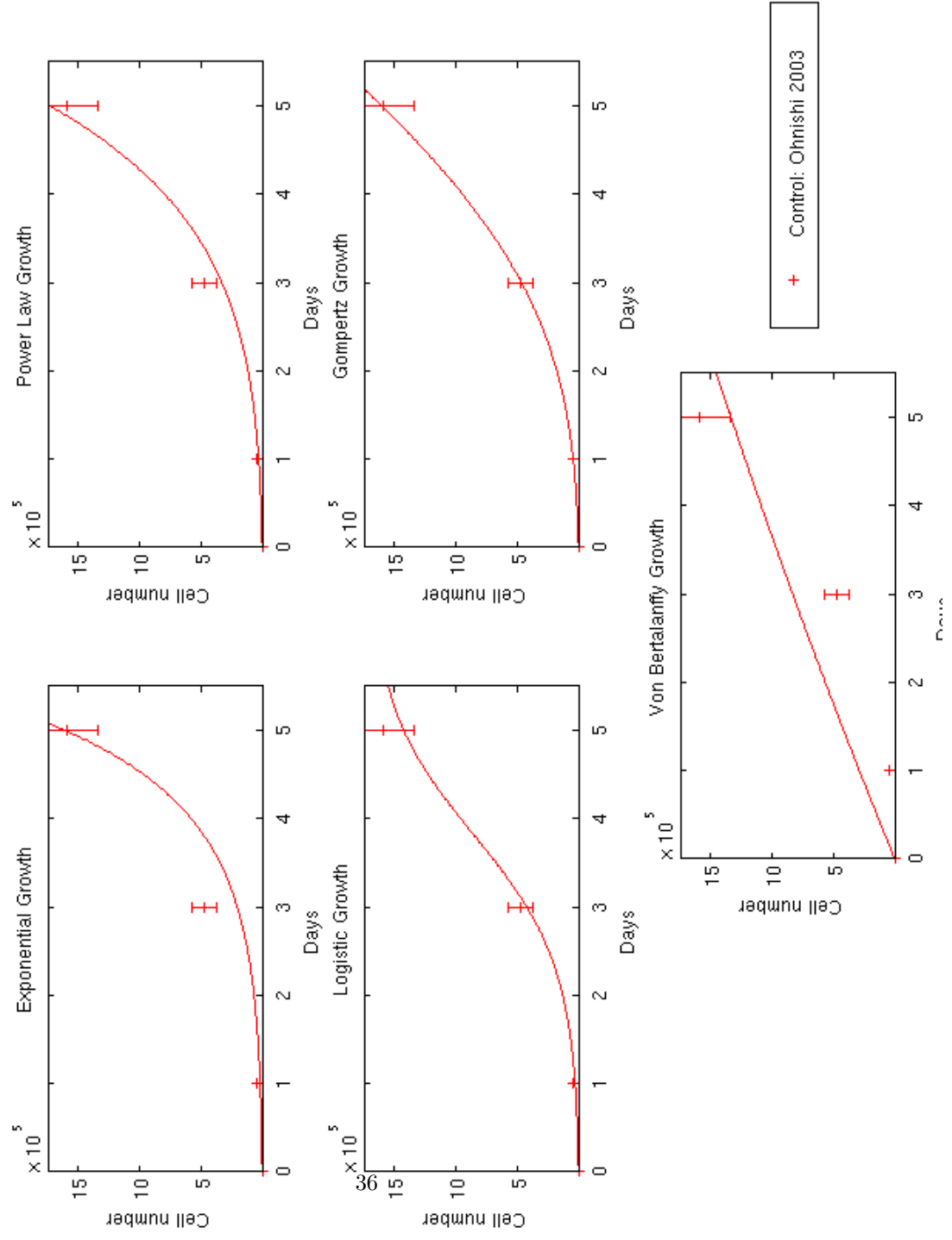


Figure Appendix C.1: Parameter Fittings to *In Vitro* Bladder Cancer Trials

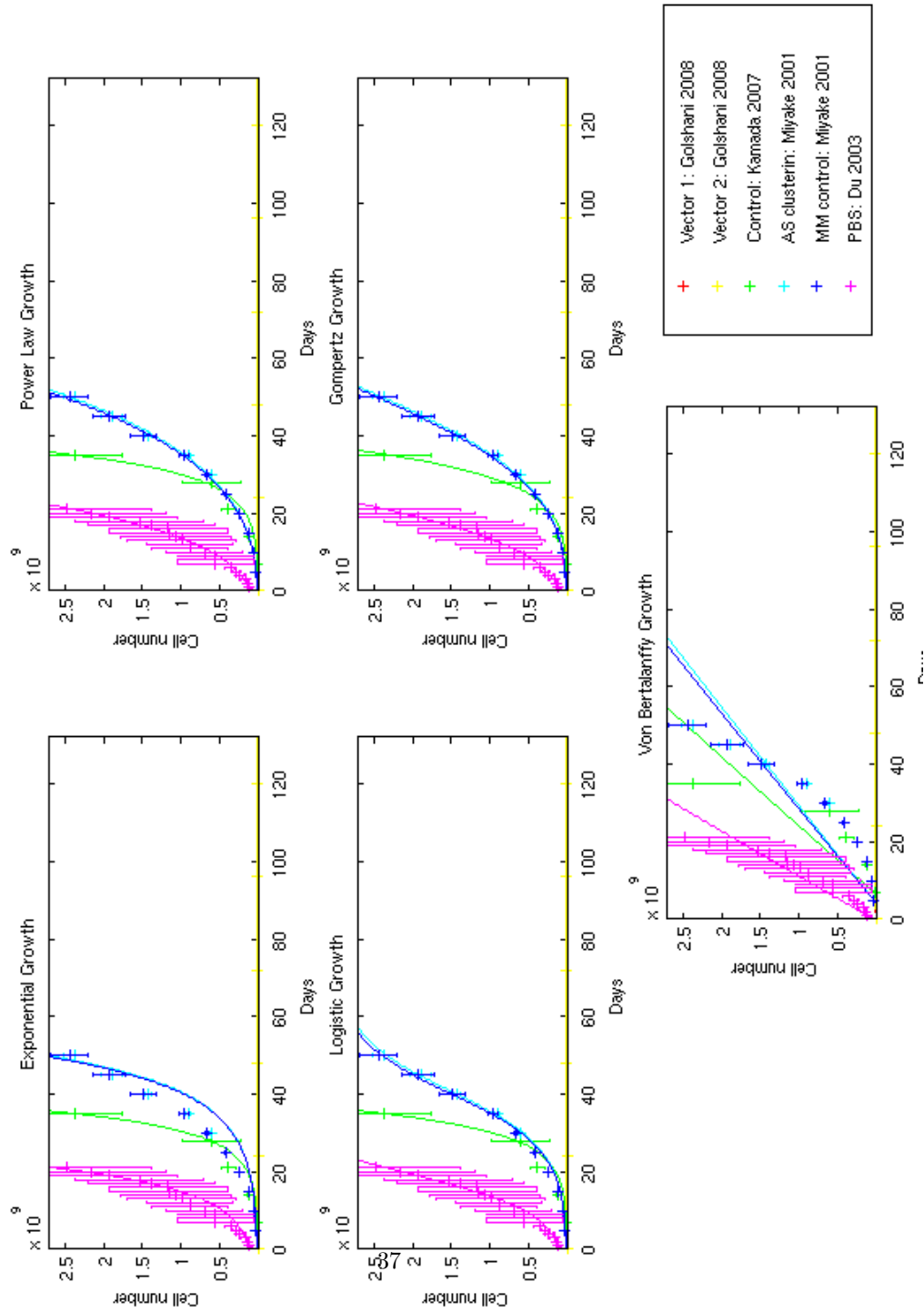


Figure Appendix C.2: Parameter Fittings to Individual *In Vivo* Bladder Cancer Trials

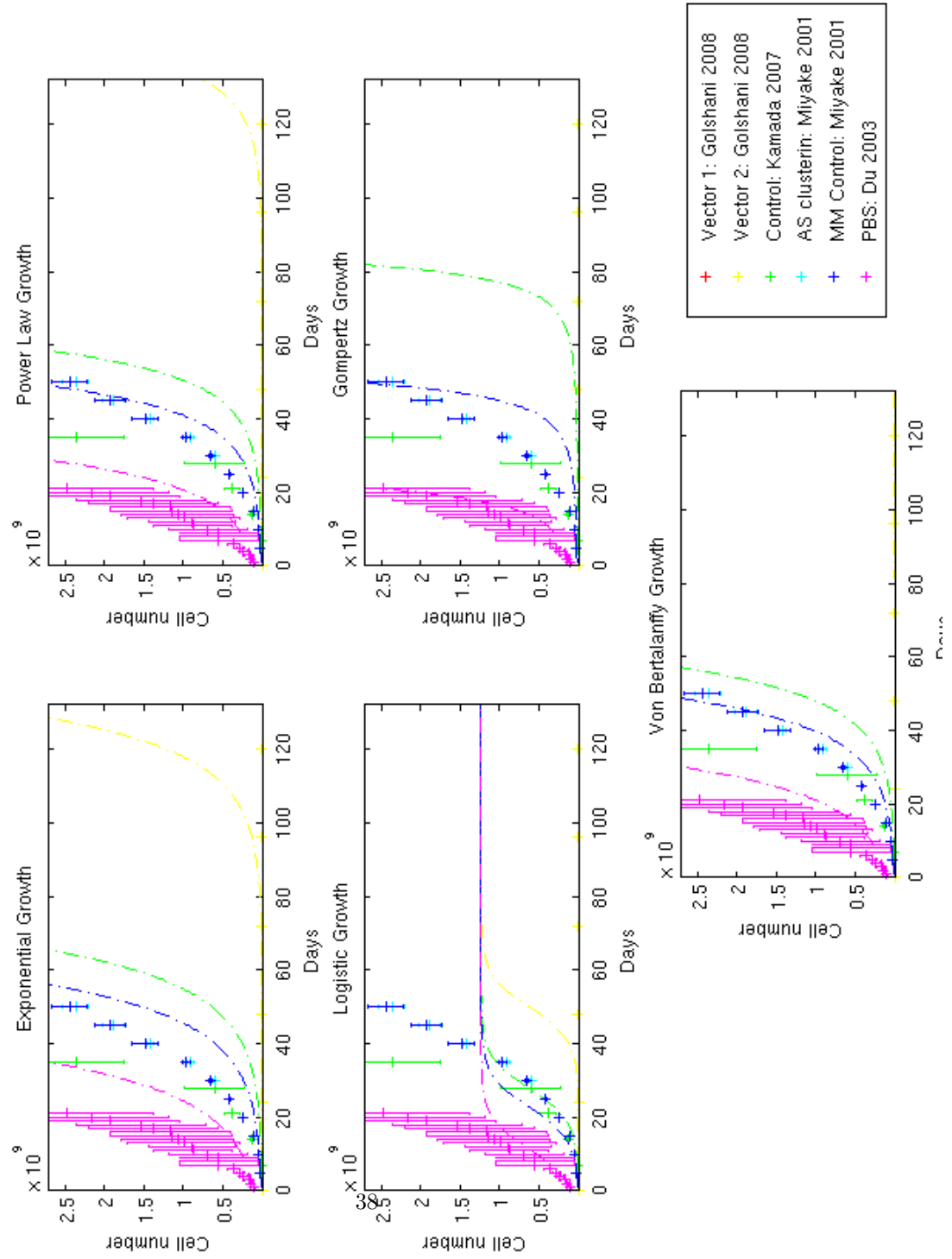


Figure Appendix C.3: Parameter Fitting to Combined *In Vivo* Bladder Cancer Trials

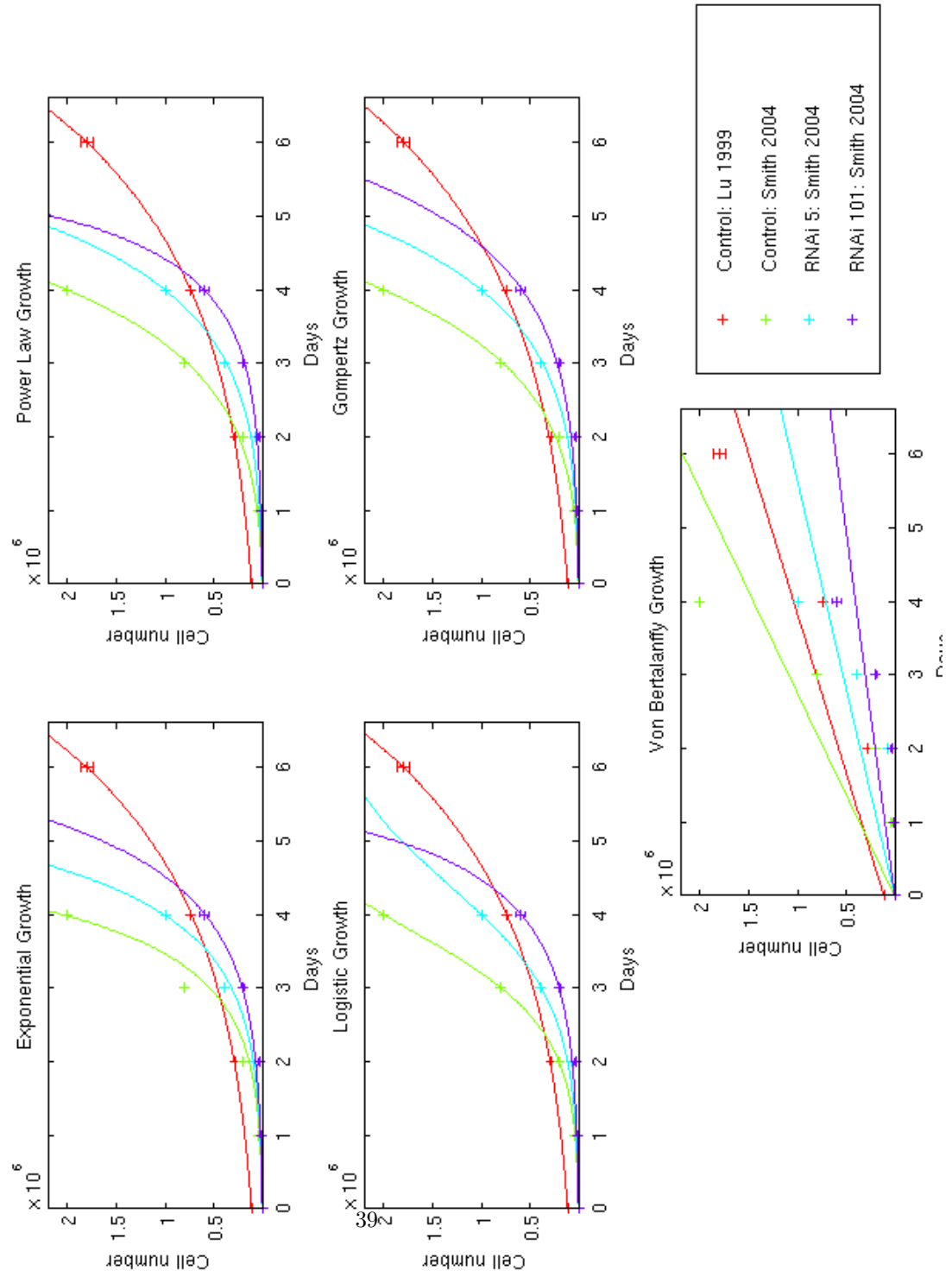


Figure Appendix C.4: Parameter Fittings to Individual *In Vitro* Breast Cancer Trials

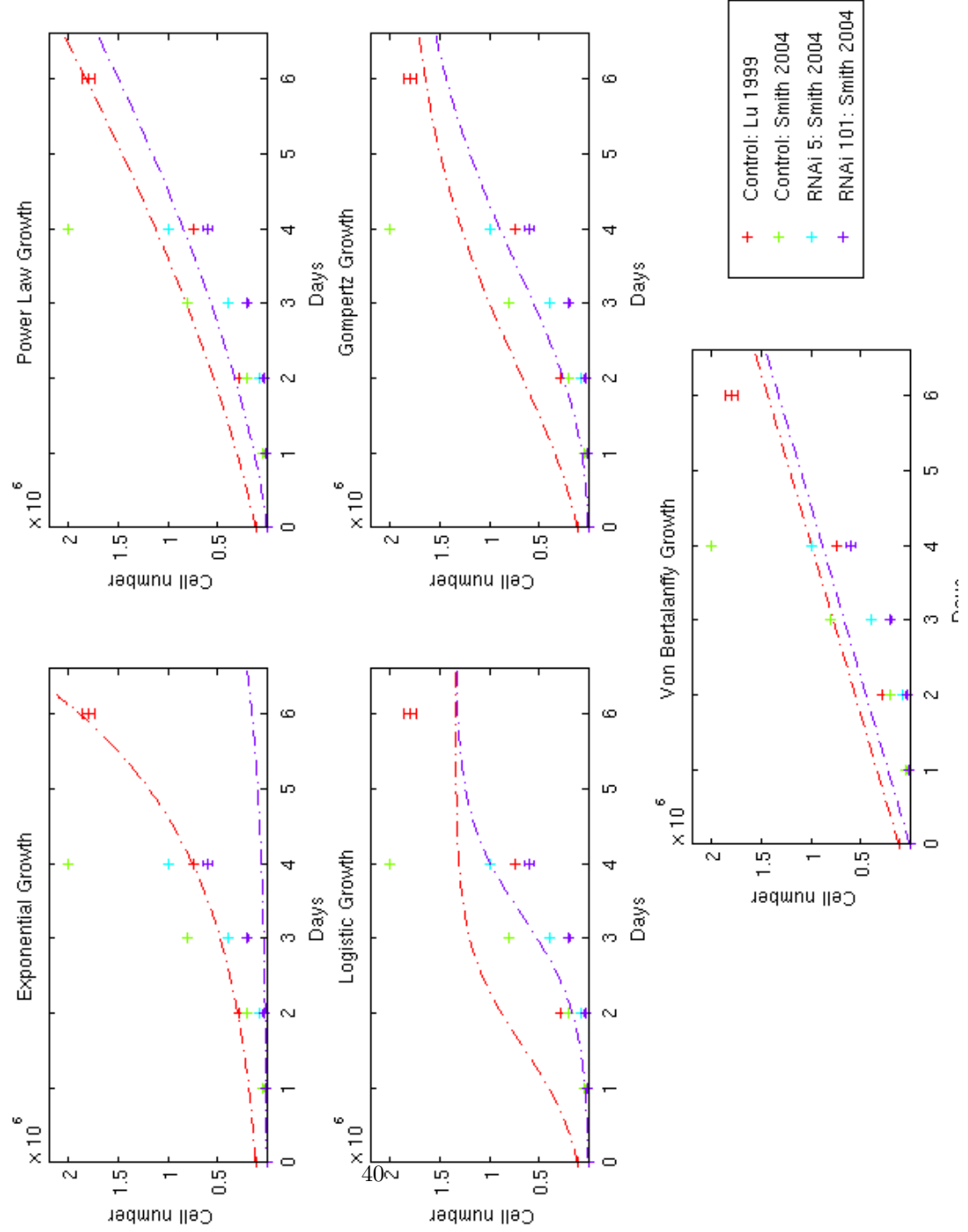


Figure Appendix C.5: Parameter Fitting to Combined *In Vitro* Breast Cancer Trials

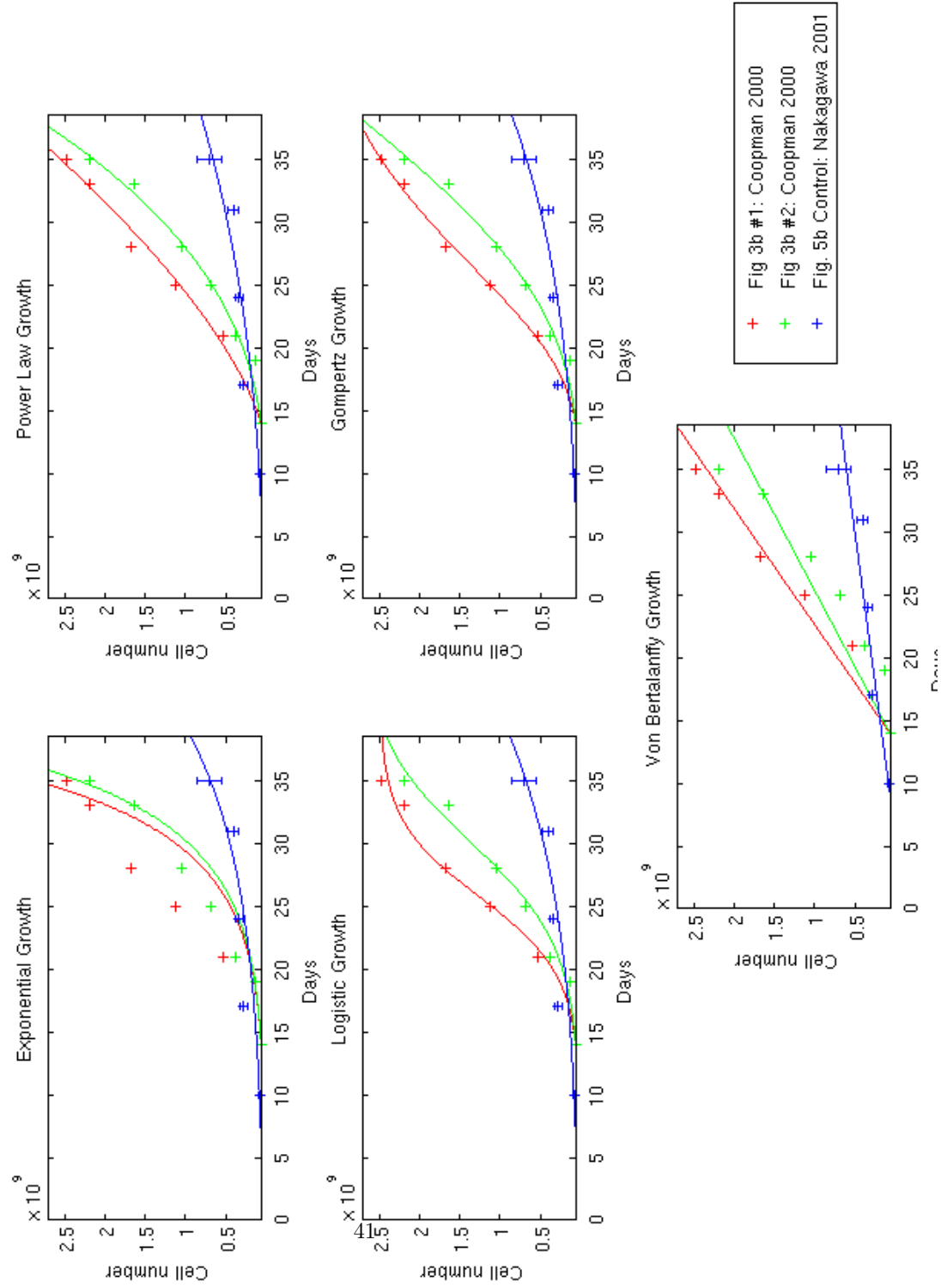


Figure Appendix C.6: Parameter Fittings to Individual *In Vivo* Breast Cancer Trials

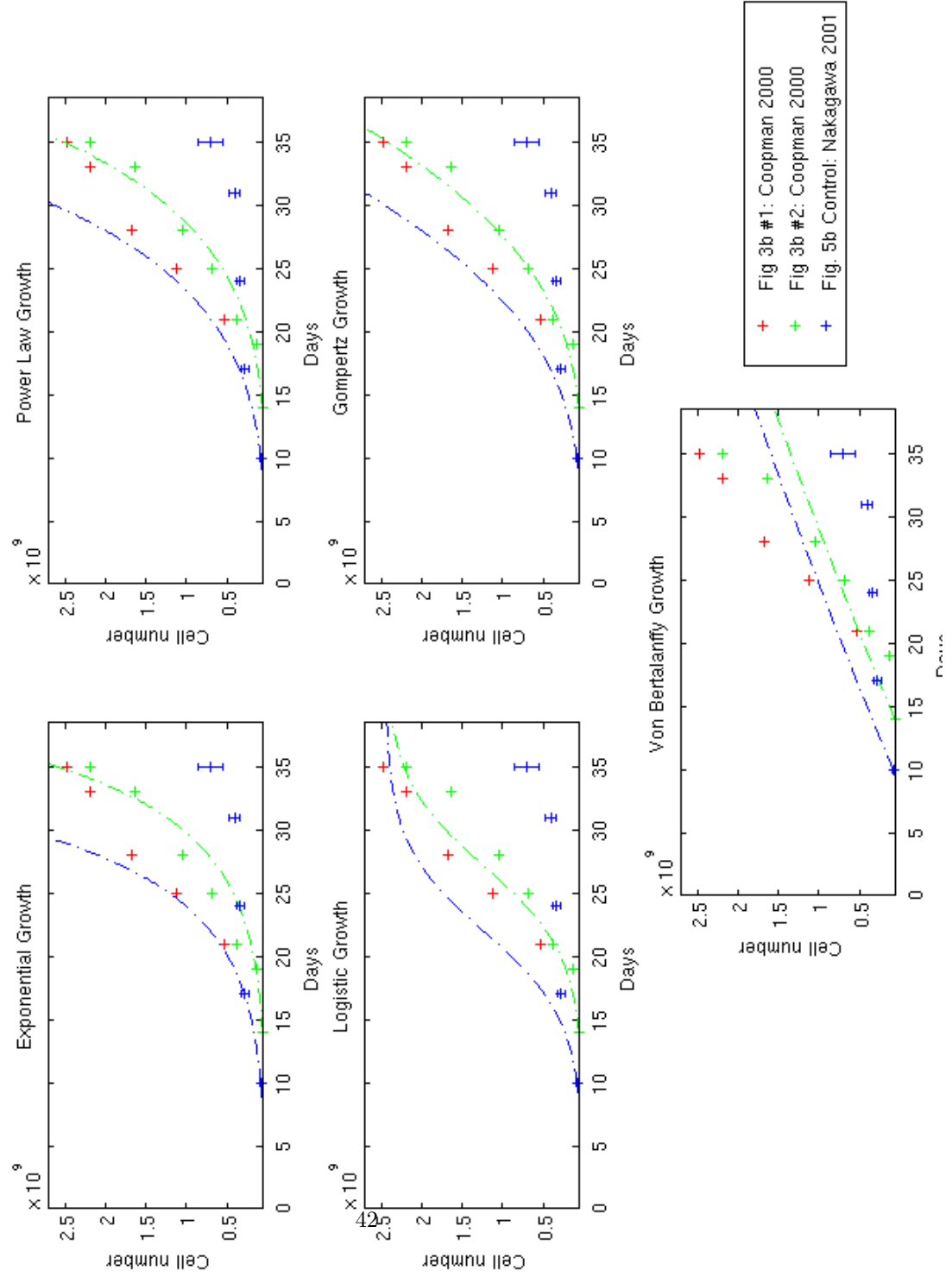


Figure Appendix C.7: Parameter Fitting to Combined *In Vivo* Breast Cancer Trials

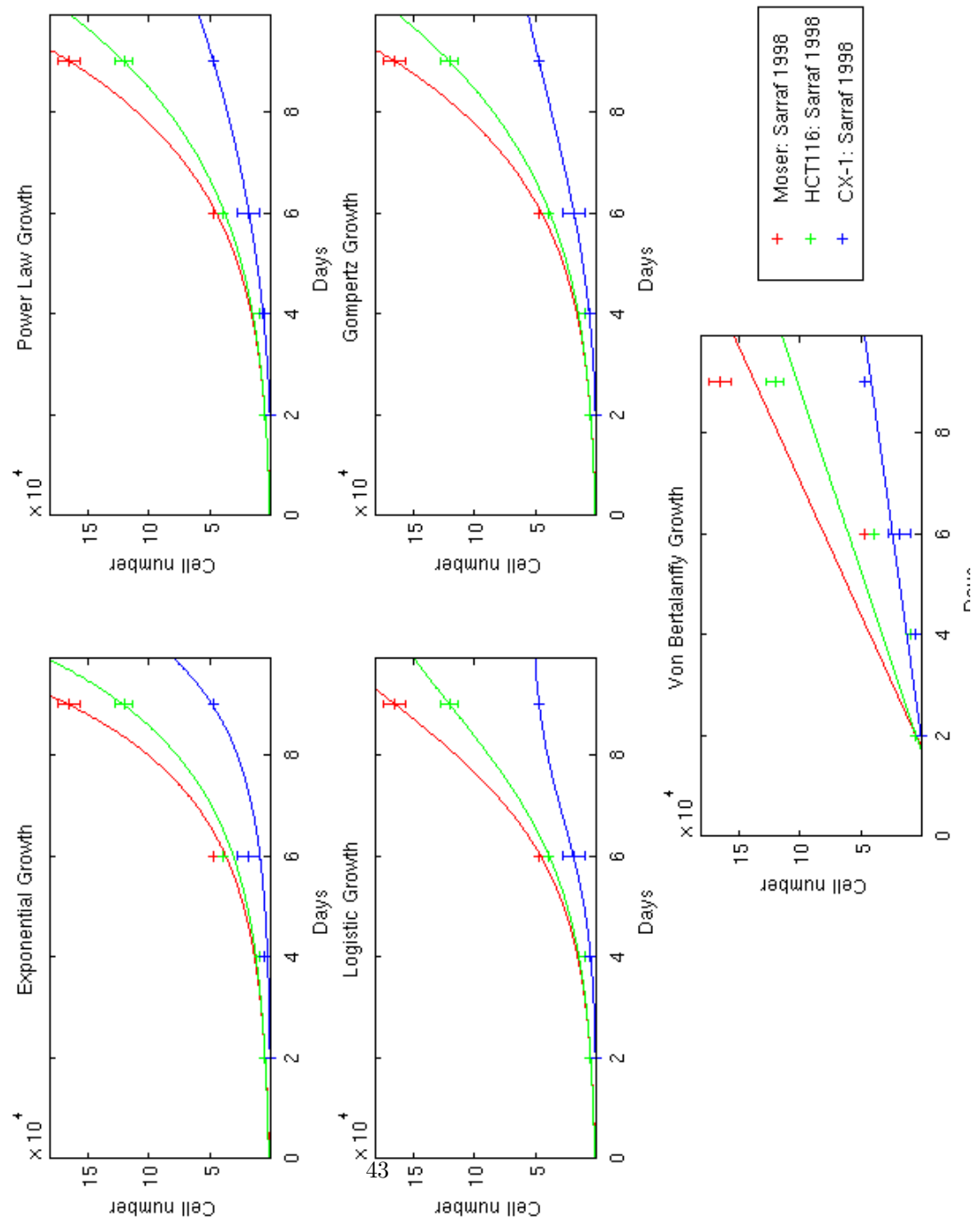


Figure Appendix C.8: Parameter Fittings to Individual *In Vitro* Colon Cancer Trials

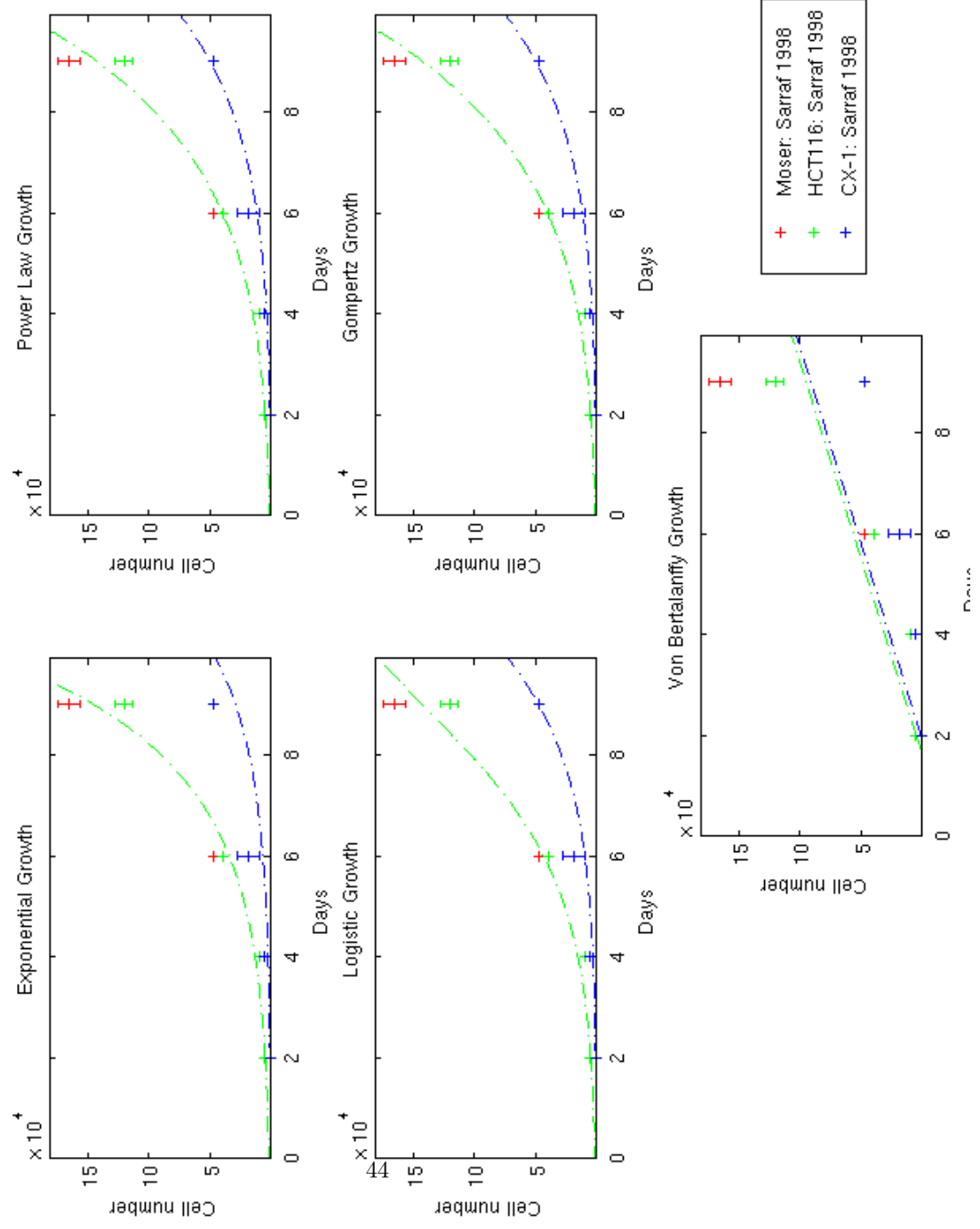


Figure Appendix C.9: Parameter Fitting to Combined *In Vitro* Colon Cancer Trials

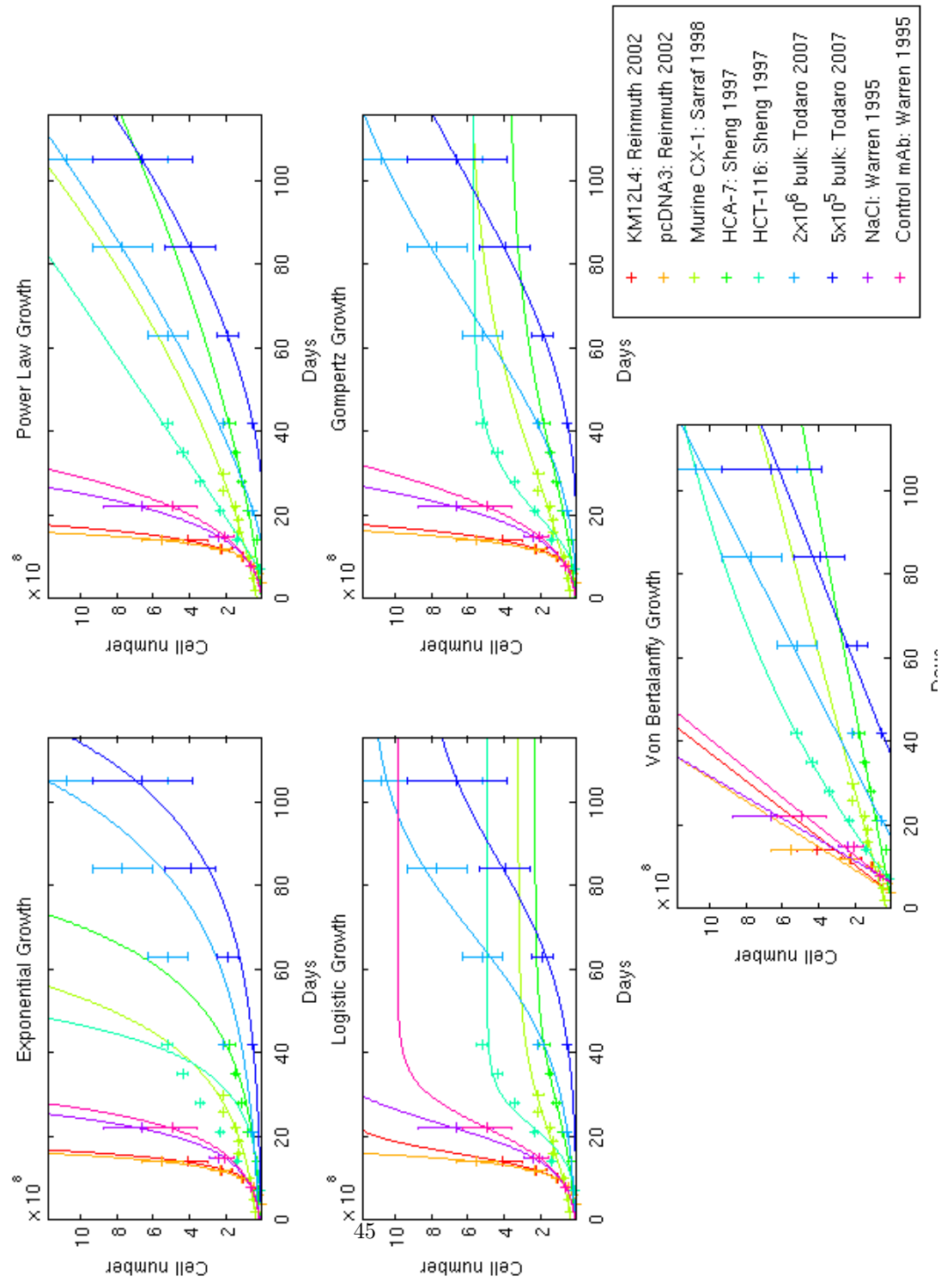


Figure Appendix C.10: Parameter Fittings to Individual *In Vivo* Colon Cancer Trials

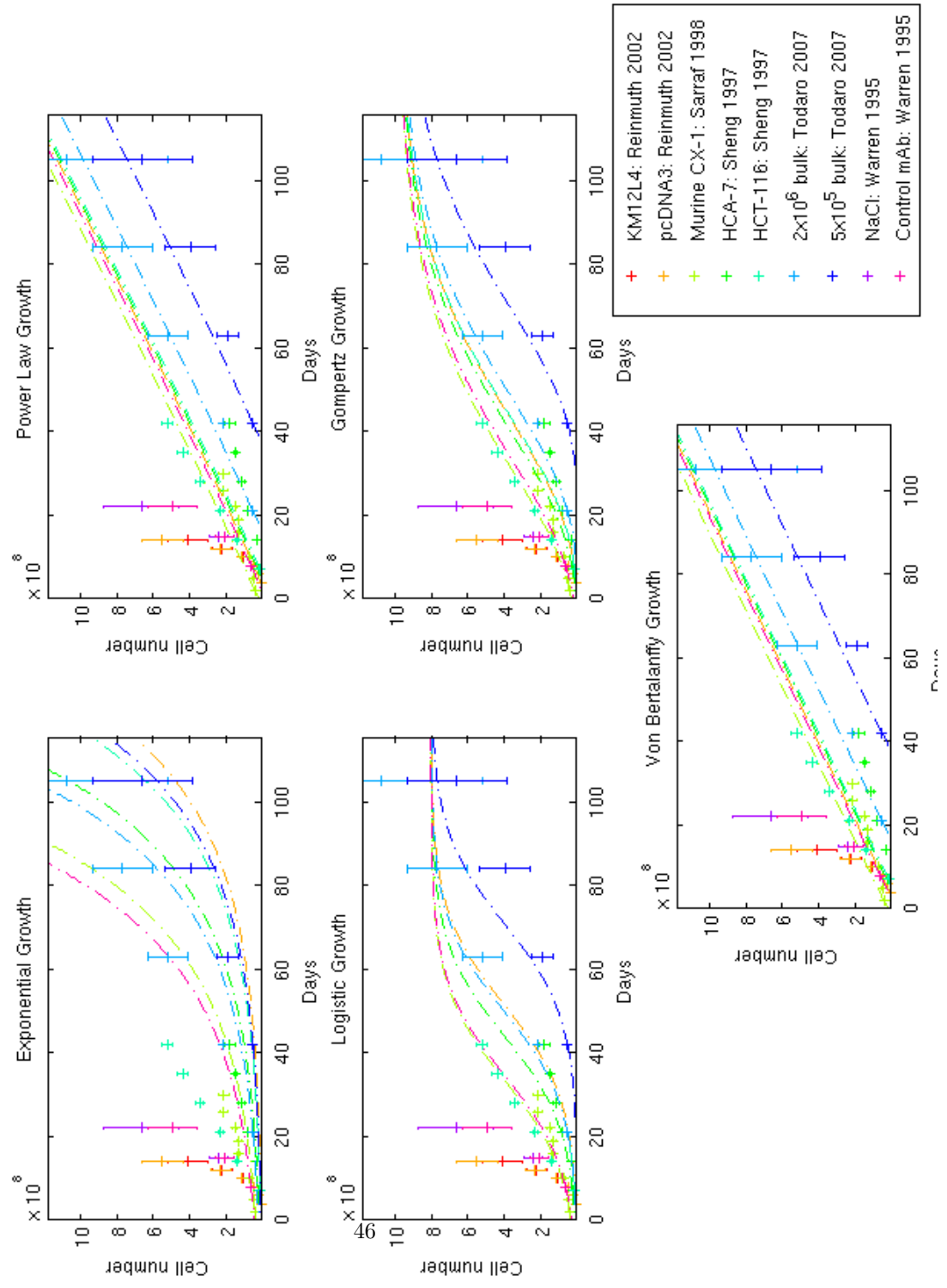


Figure Appendix C.11: Parameter Fitting to Combined *In Vivo* Colon Cancer Trials

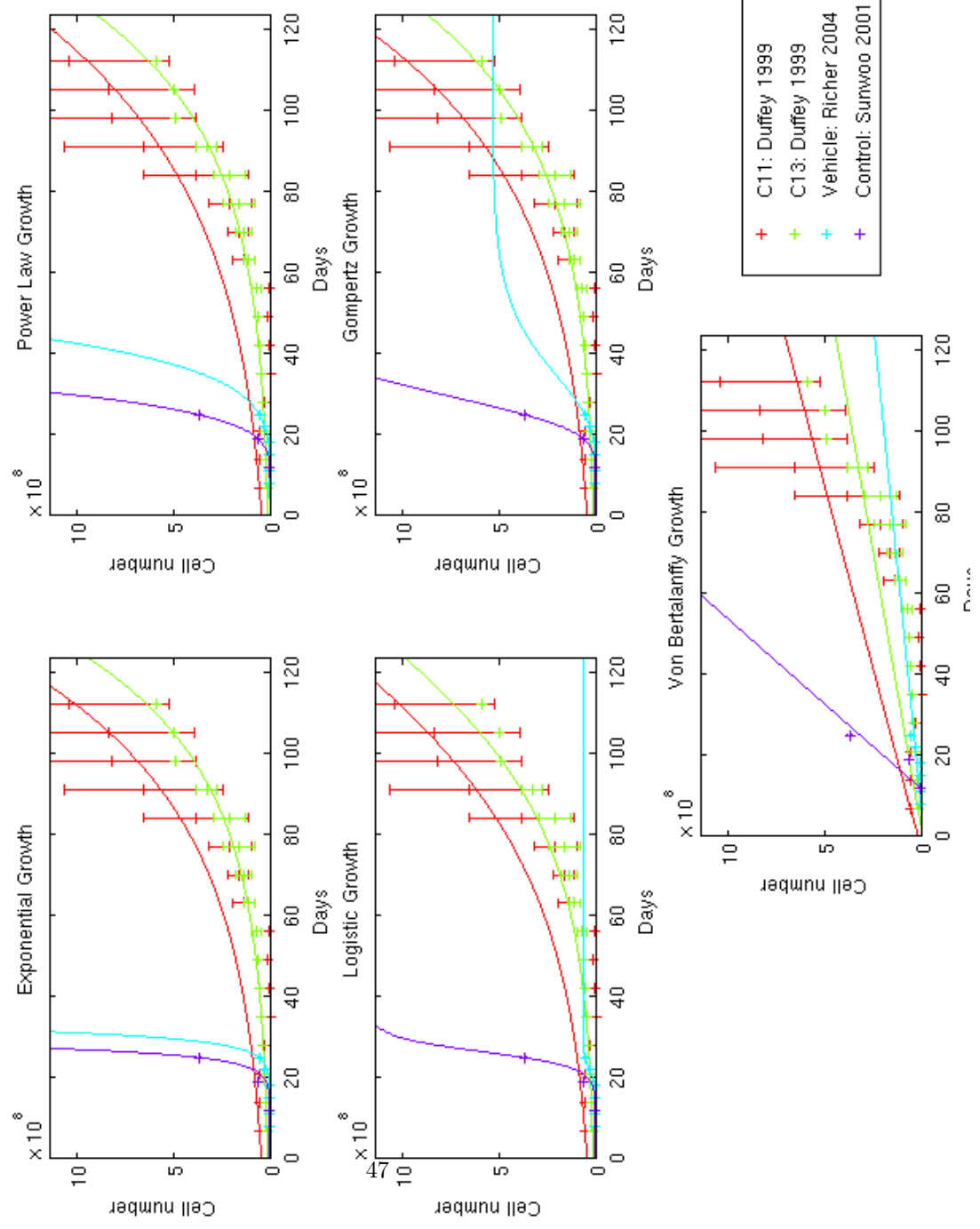


Figure Appendix C.12: Parameter Fittings to Individual *In Vitro* Head and Neck Squamous Cell Carcinoma Trials

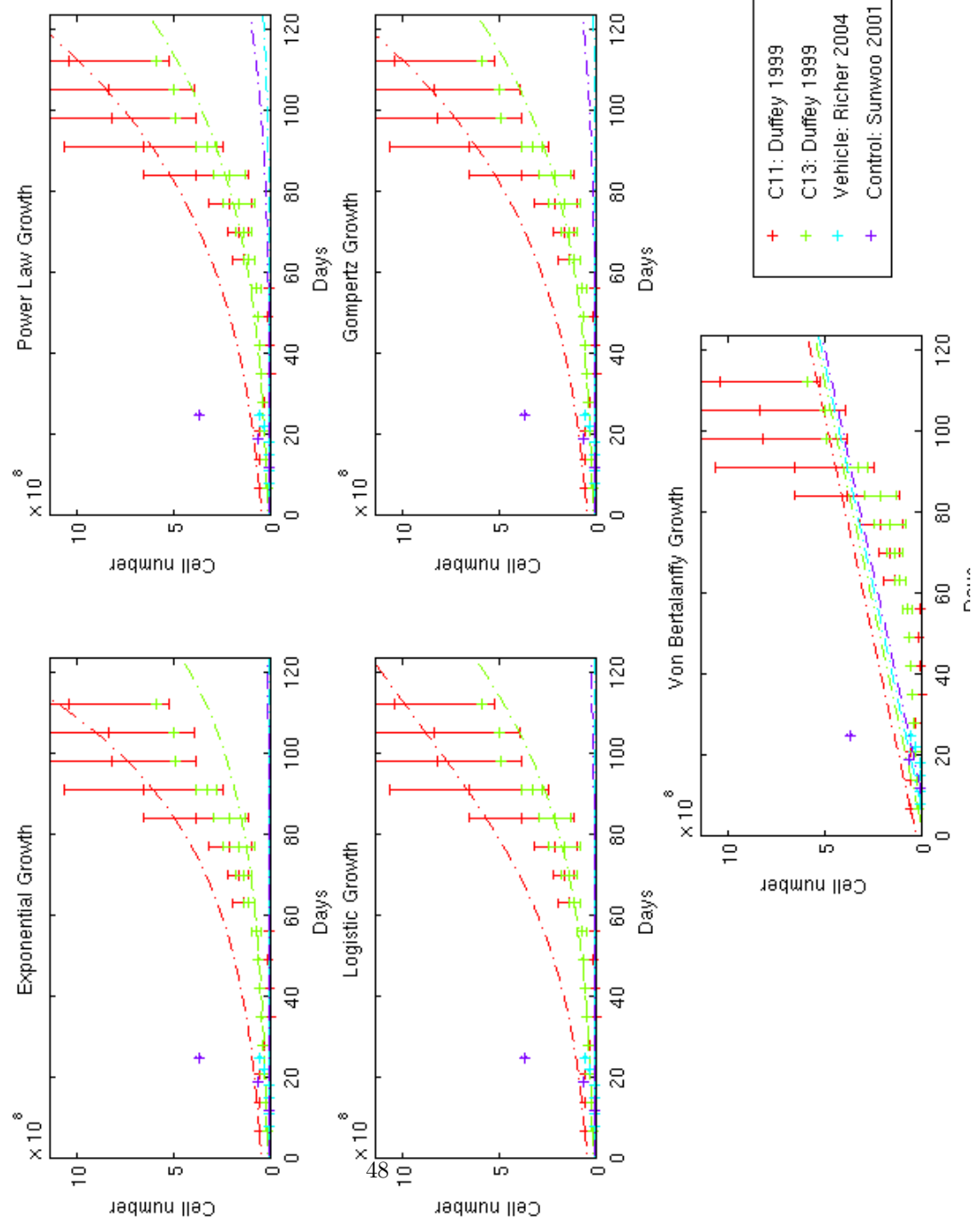


Figure Appendix C.13: Parameter Fitting to Combined *In Vitro* Head and Neck Squamous Cell Carcinoma Trials

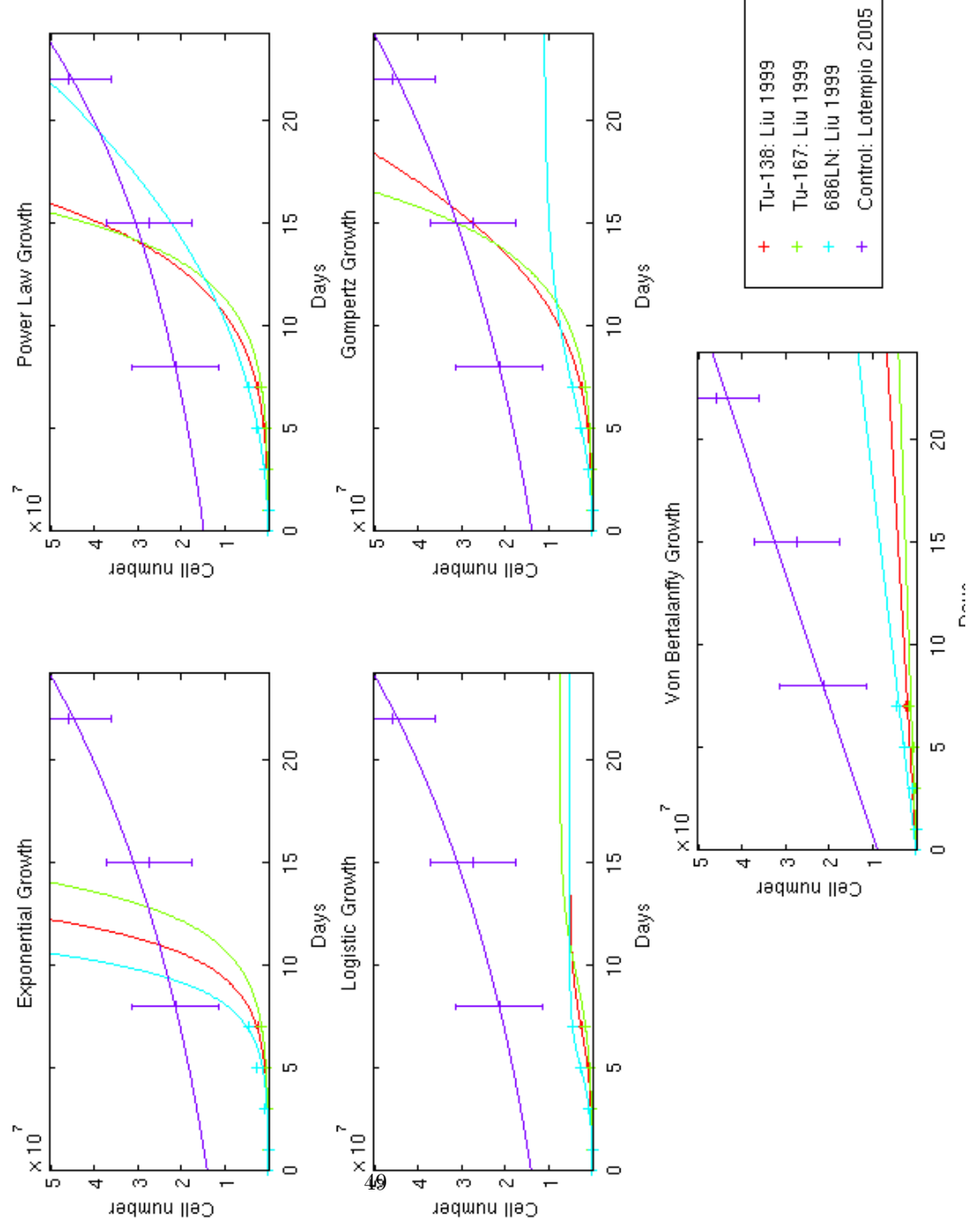


Figure Appendix C.14: Parameter Fittings to Individual *In Vivo* Head and Neck Squamous Cell Carcinoma Trials

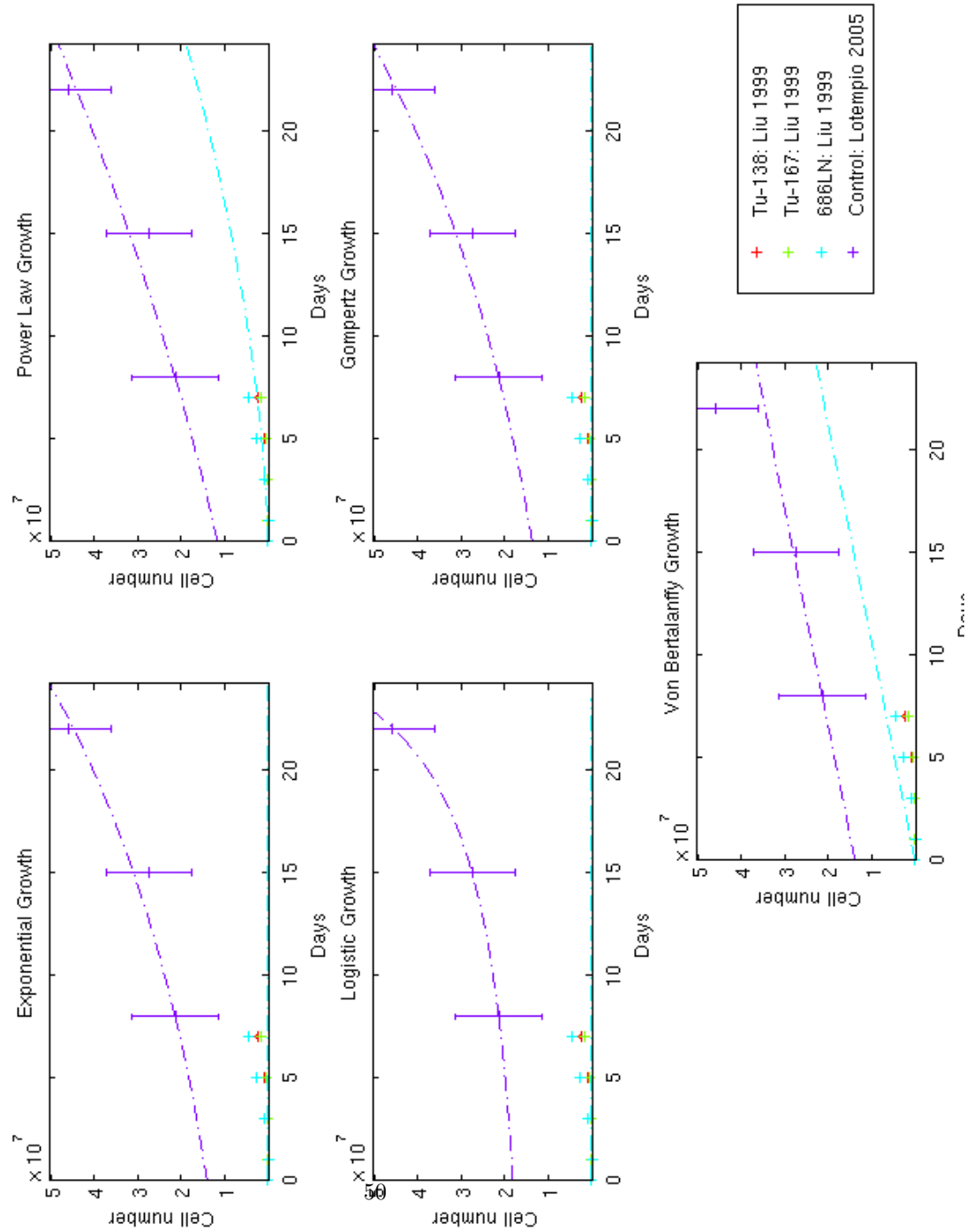


Figure Appendix C.15: Parameter Fitting to Combined *In Vivo* Head and Neck Squamous Cell Carcinoma Trials

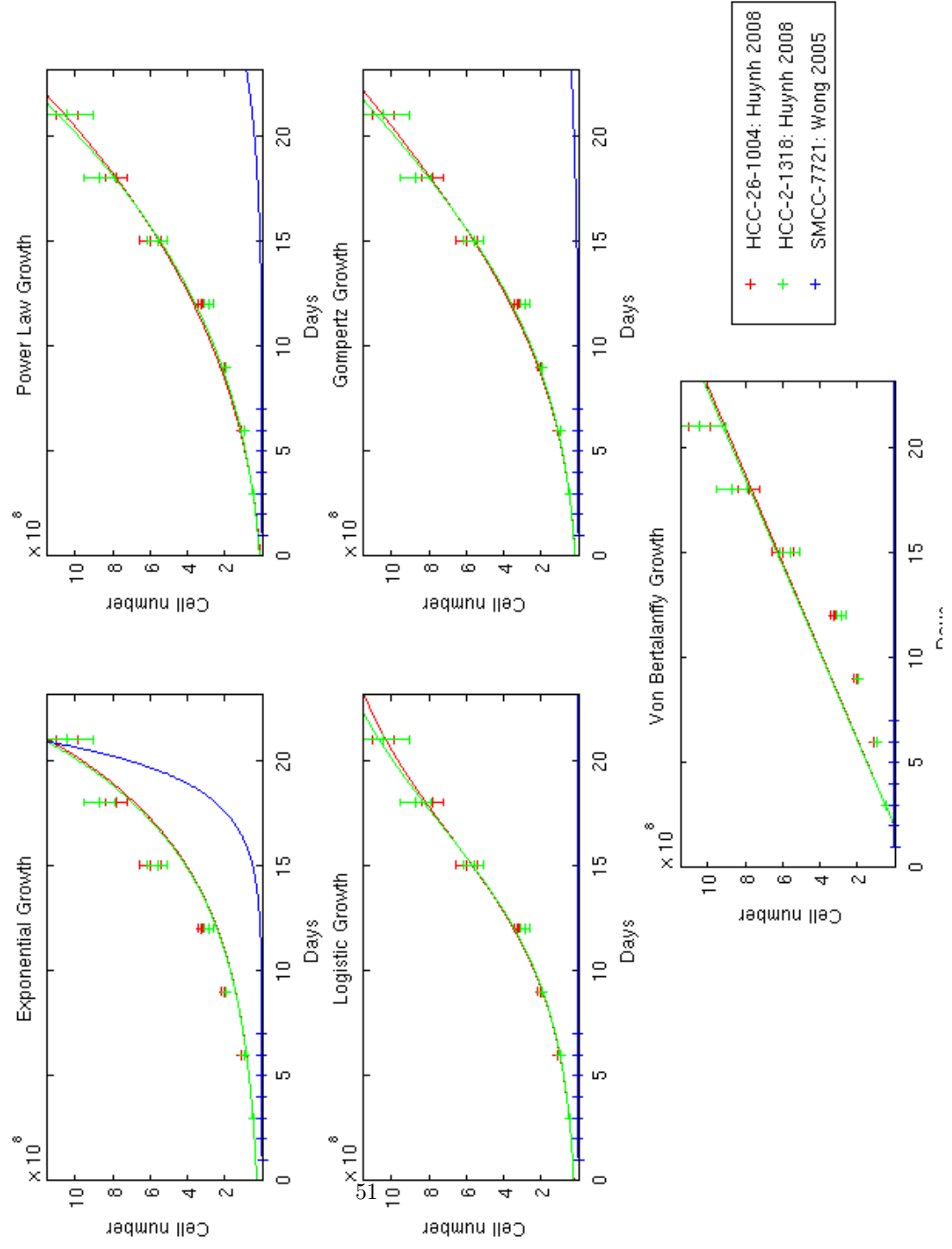


Figure Appendix C.16: Parameter Fittings to Individual *In Vitro* Hepatocellular Carcinoma Trials

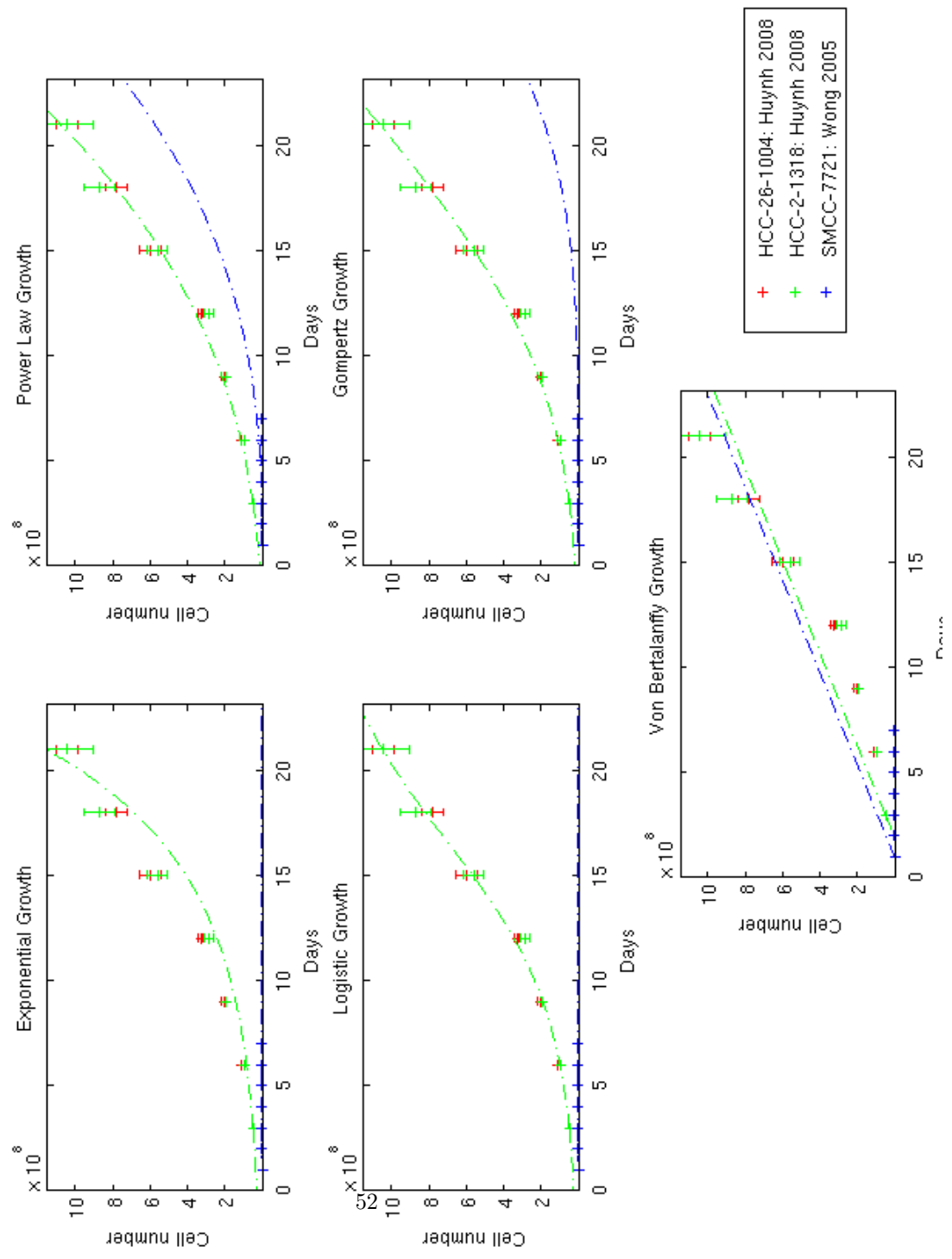


Figure Appendix C.17: Parameter Fitting to Combined *In Vitro* Hepatocellular Carcinoma Trials

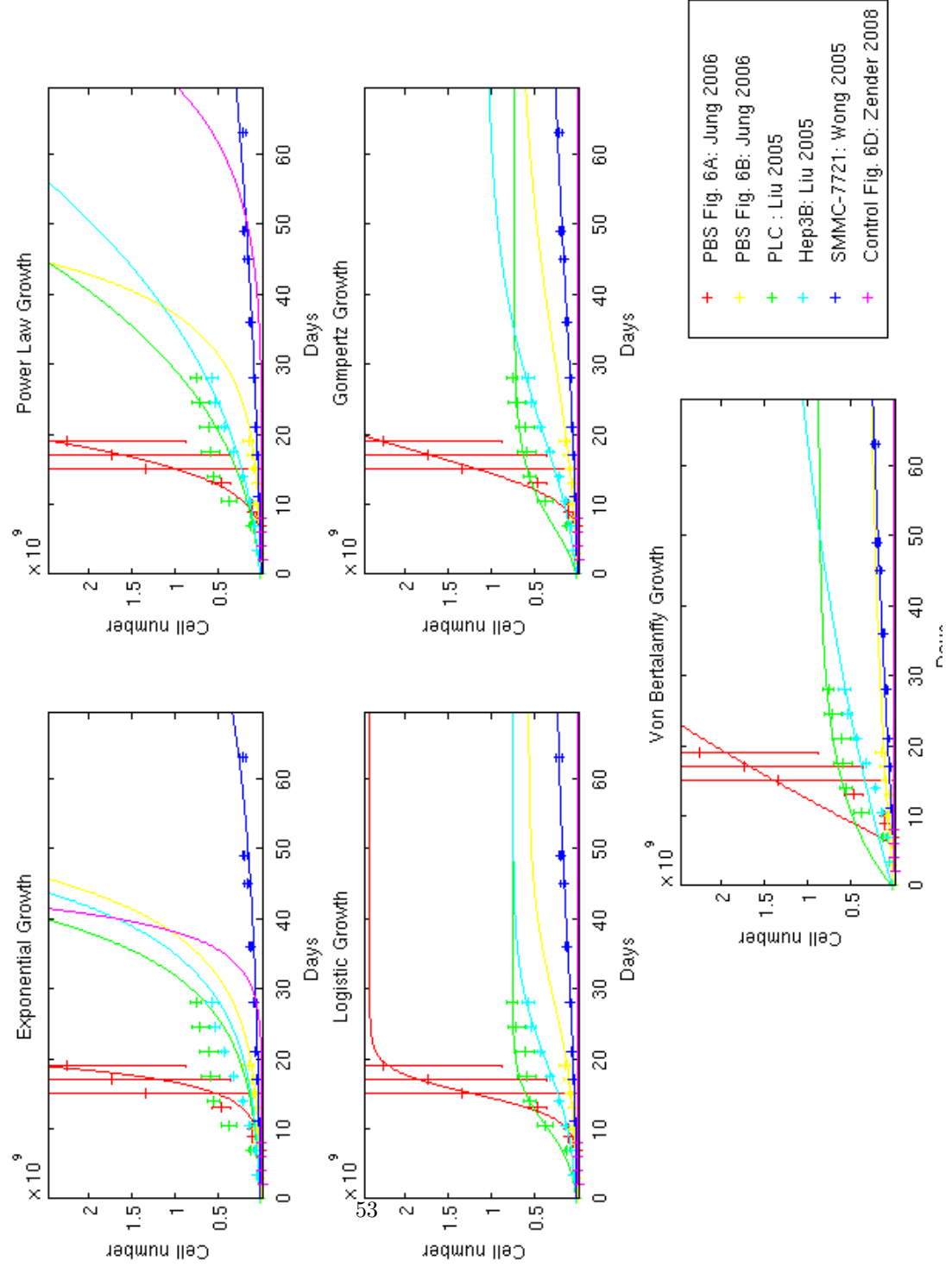


Figure Appendix C.18: Parameter Fittings to Individual *In Vivo* Hepatocellular Carcinoma Trials

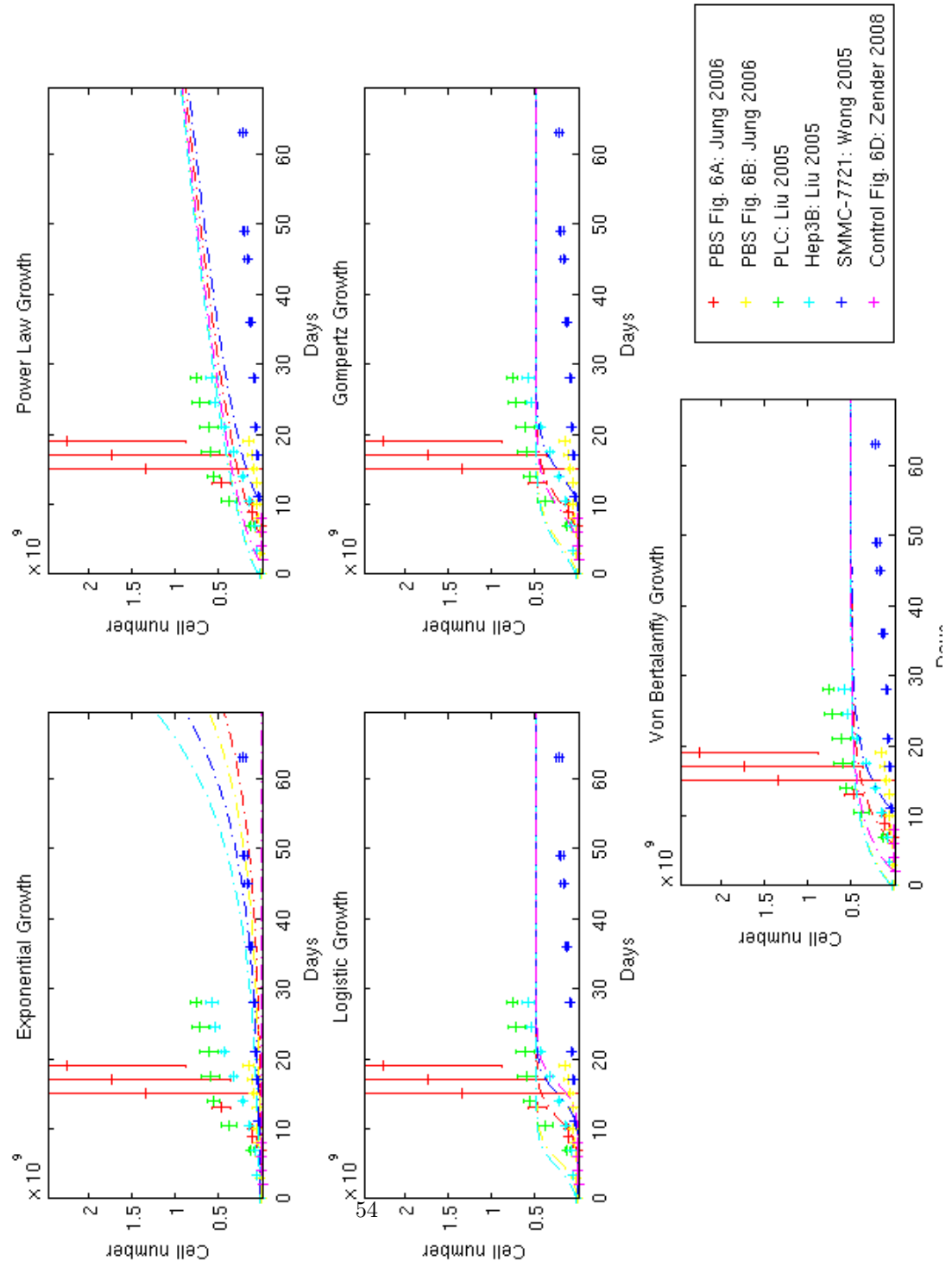


Figure Appendix C.19: Parameter Fitting to Combined *In Vivo* Hepatocellular Carcinoma Trials

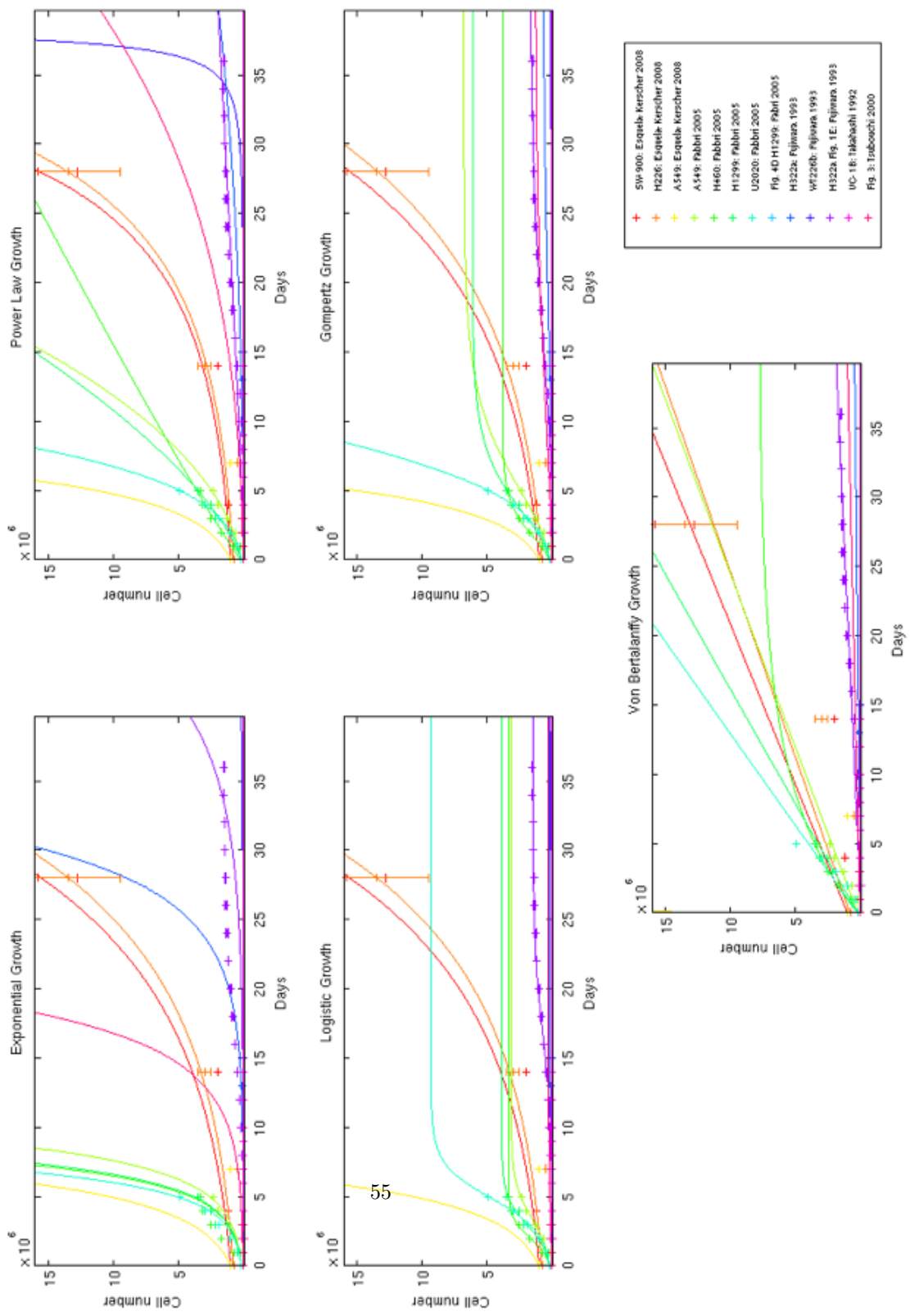


Figure Appendix C.20: Parameter Fittings to Individual *In Vitro* Lung Cancer Trials

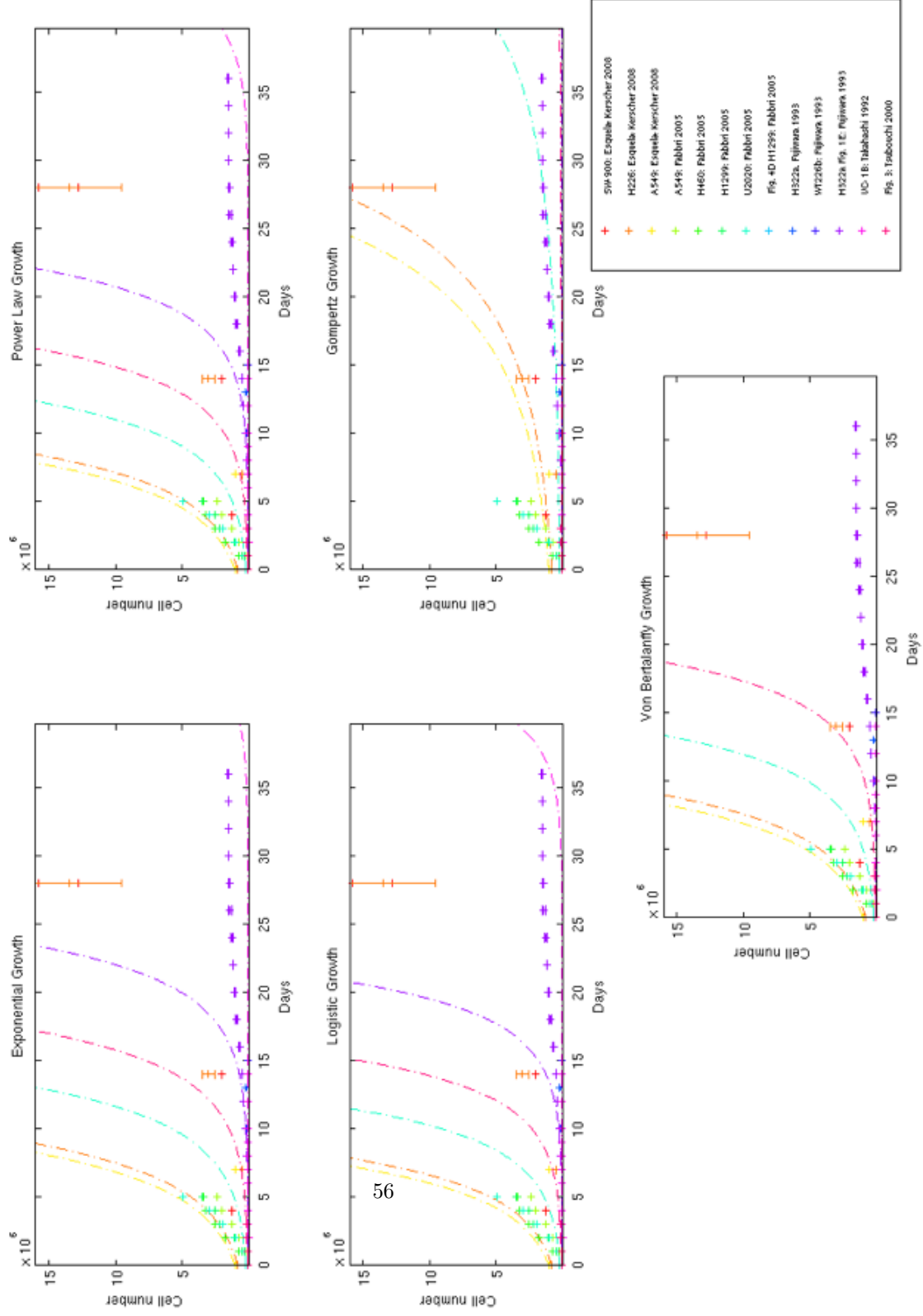


Figure Appendix C.21: Parameter Fitting to Combined *In Vitro* Lung Cancer Trials

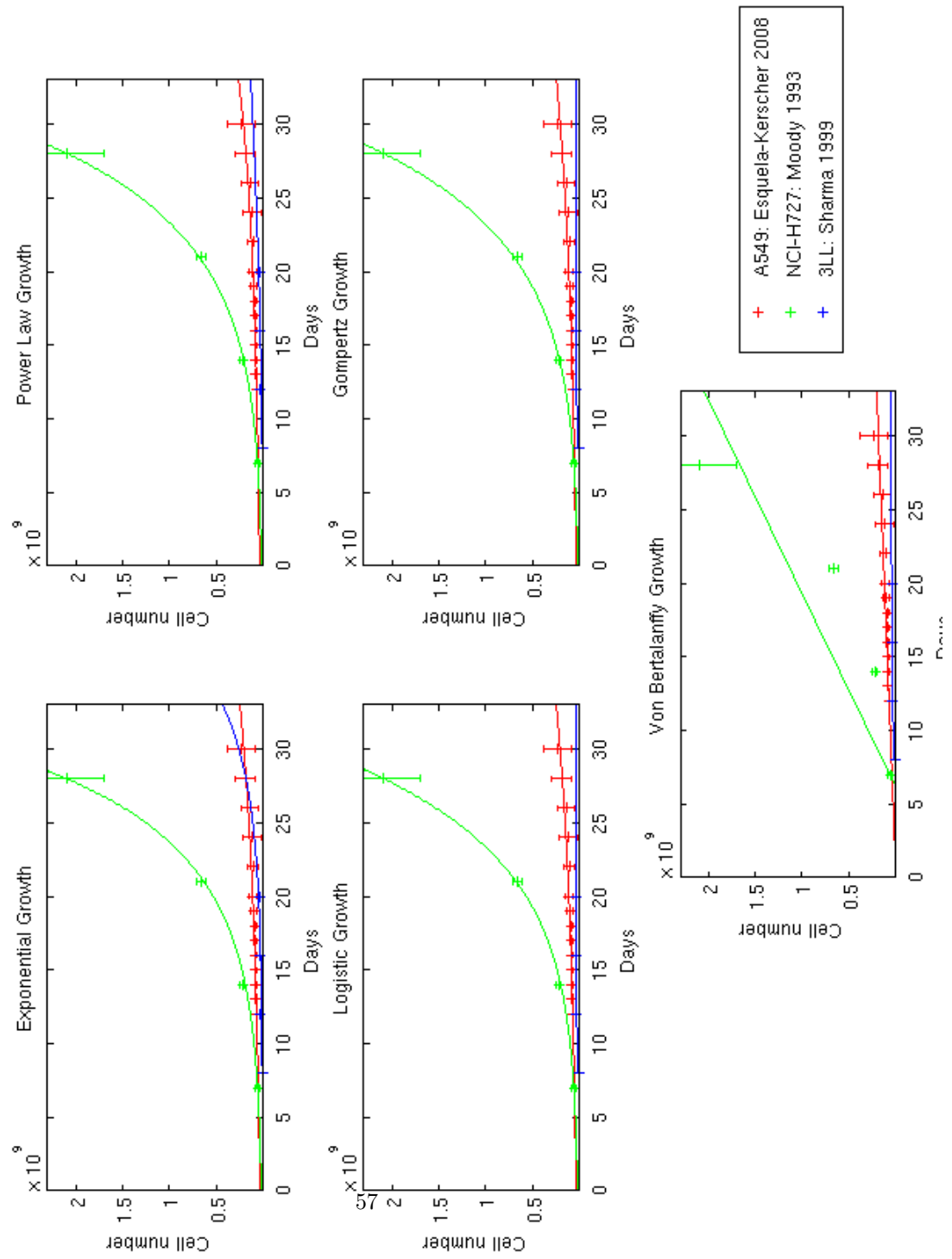


Figure Appendix C.22: Parameter Fittings to Individual *In Vivo* Lung Cancer Trials

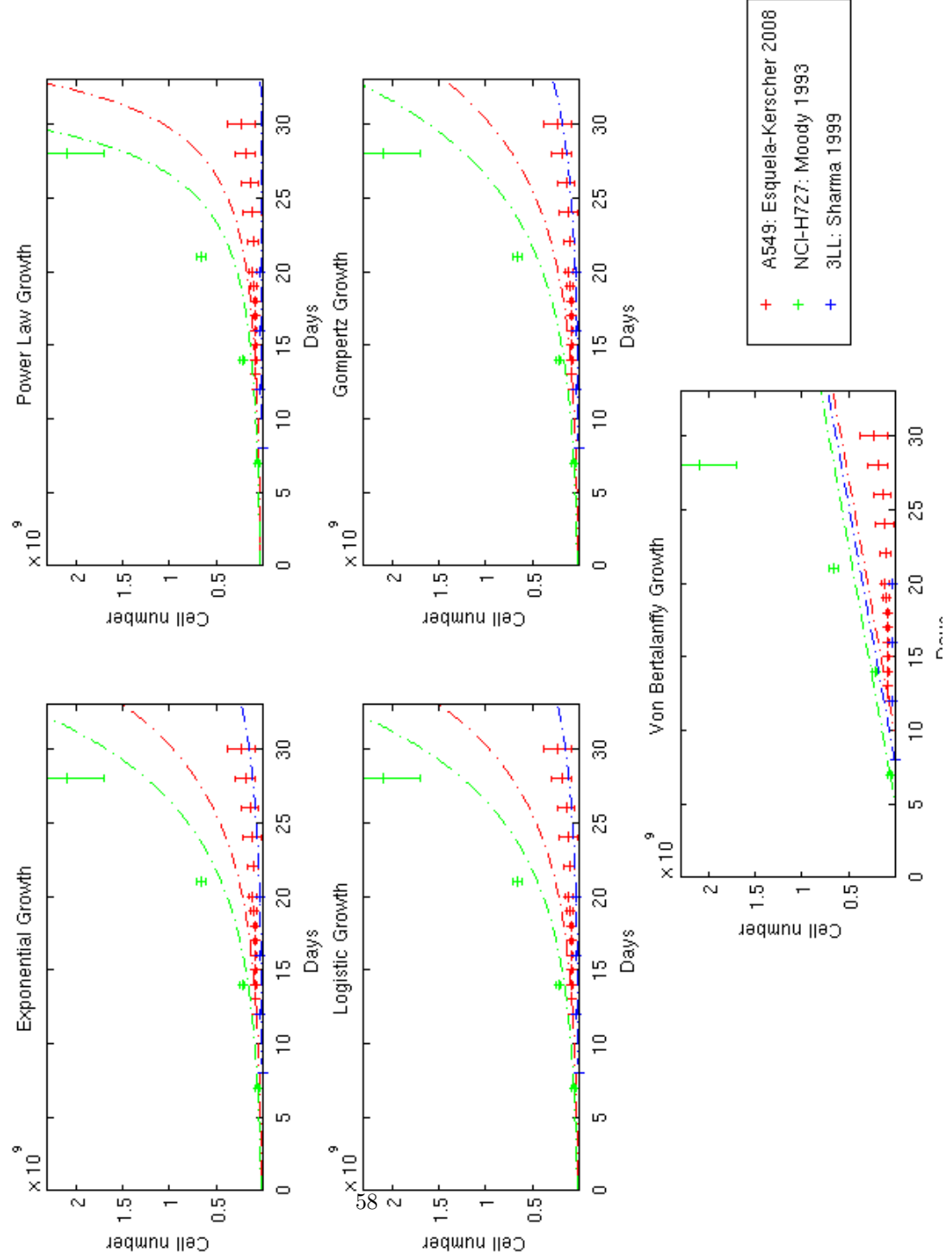


Figure Appendix C.23: Parameter Fitting to Combined *In Vivo* Lung Cancer Trials

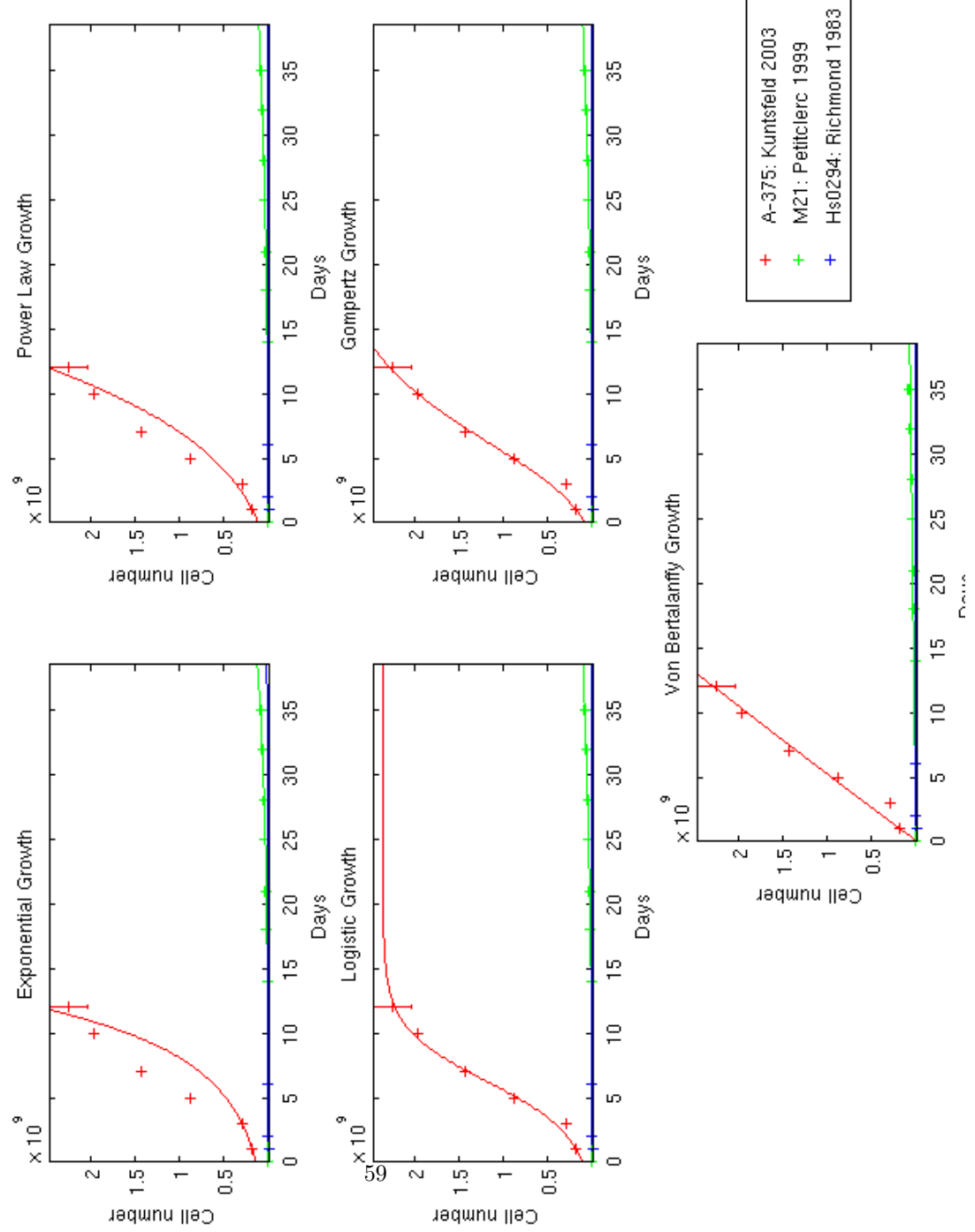


Figure Appendix C.24: Parameter Fittings to Individual *In Vitro* Melanoma Trials

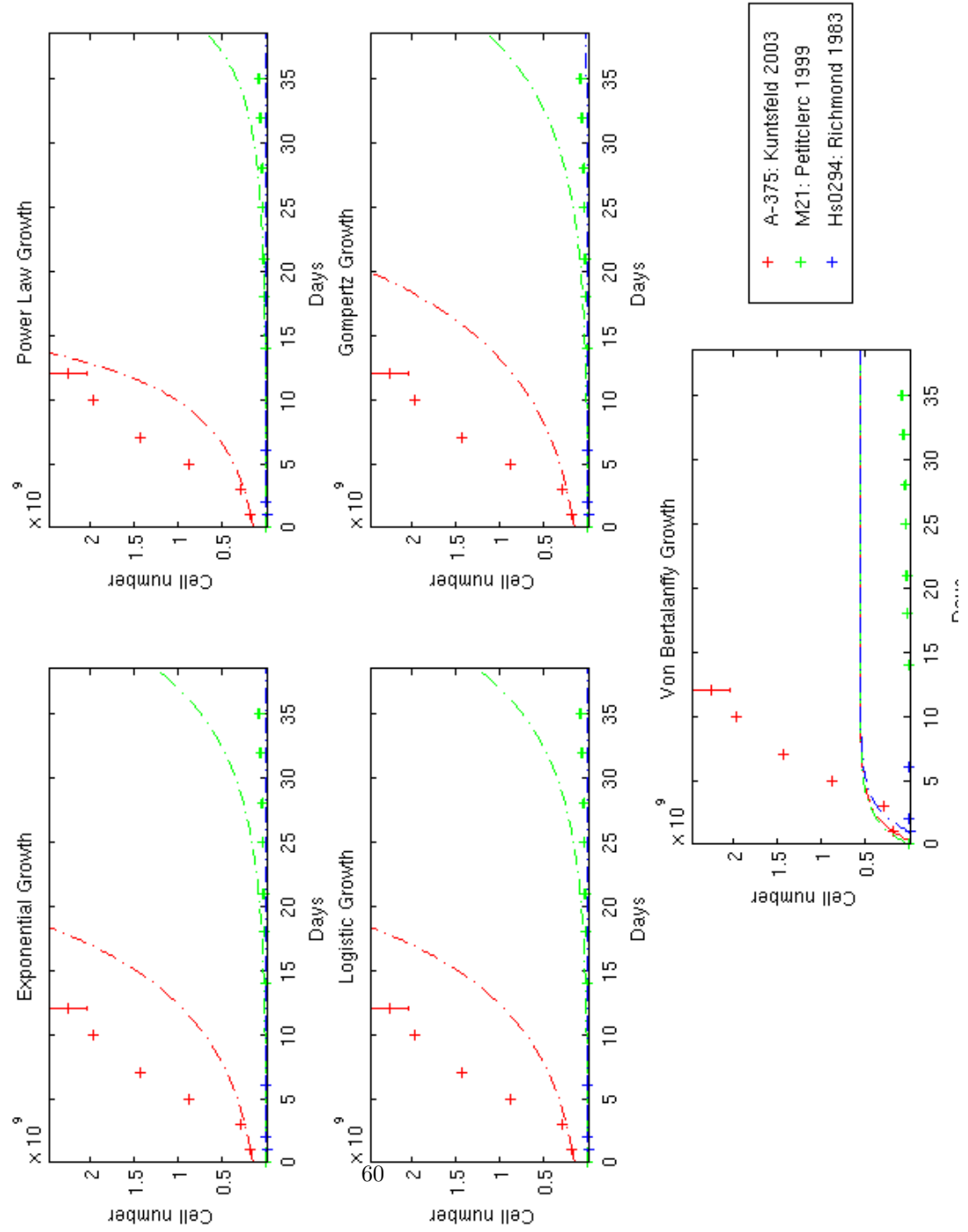


Figure Appendix C.25: Parameter Fitting to Combined *In Vitro* Melanoma Trials

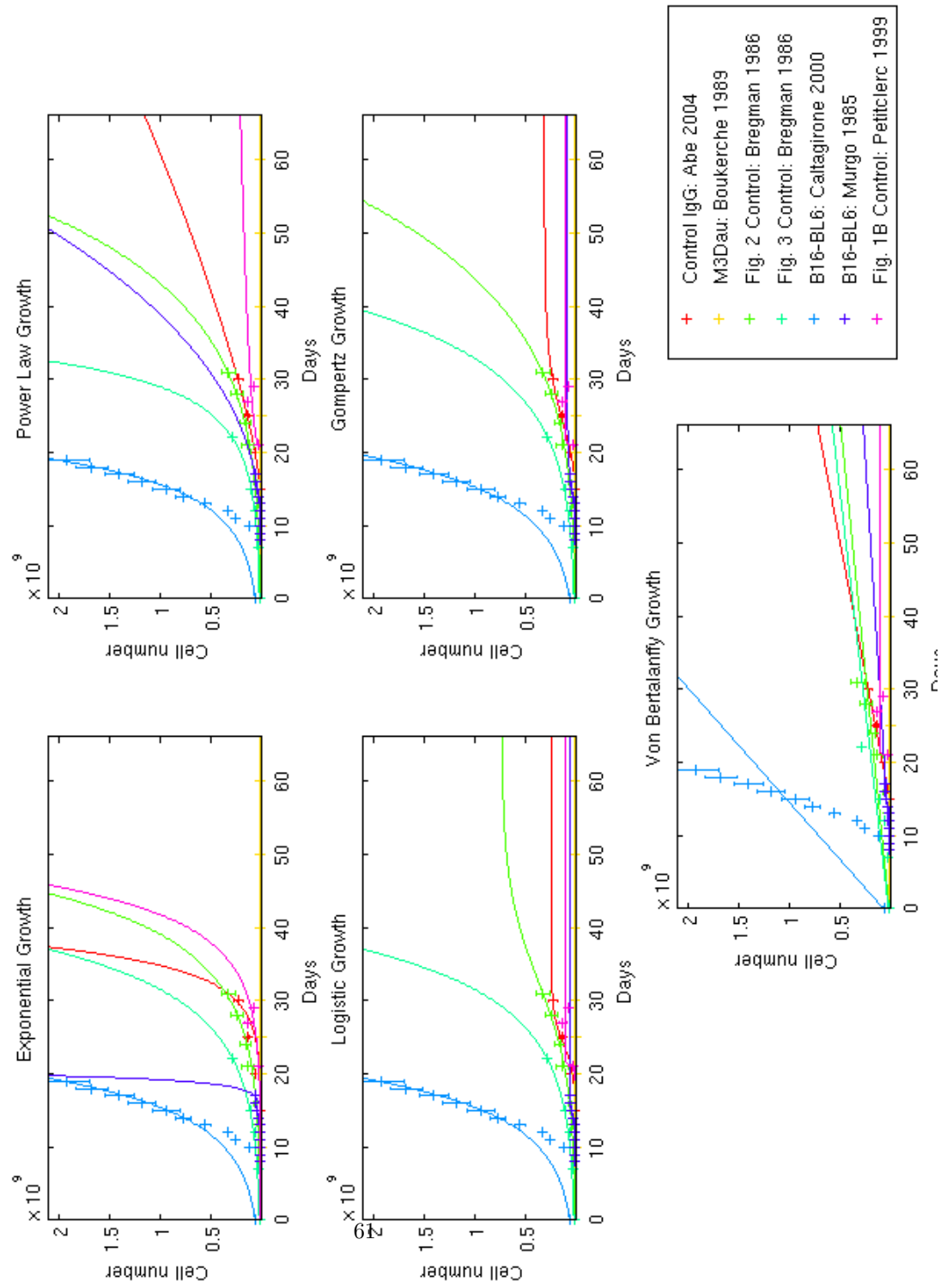


Figure Appendix C.26: Parameter Fittings to Individual *In Vivo* Melanoma Trials

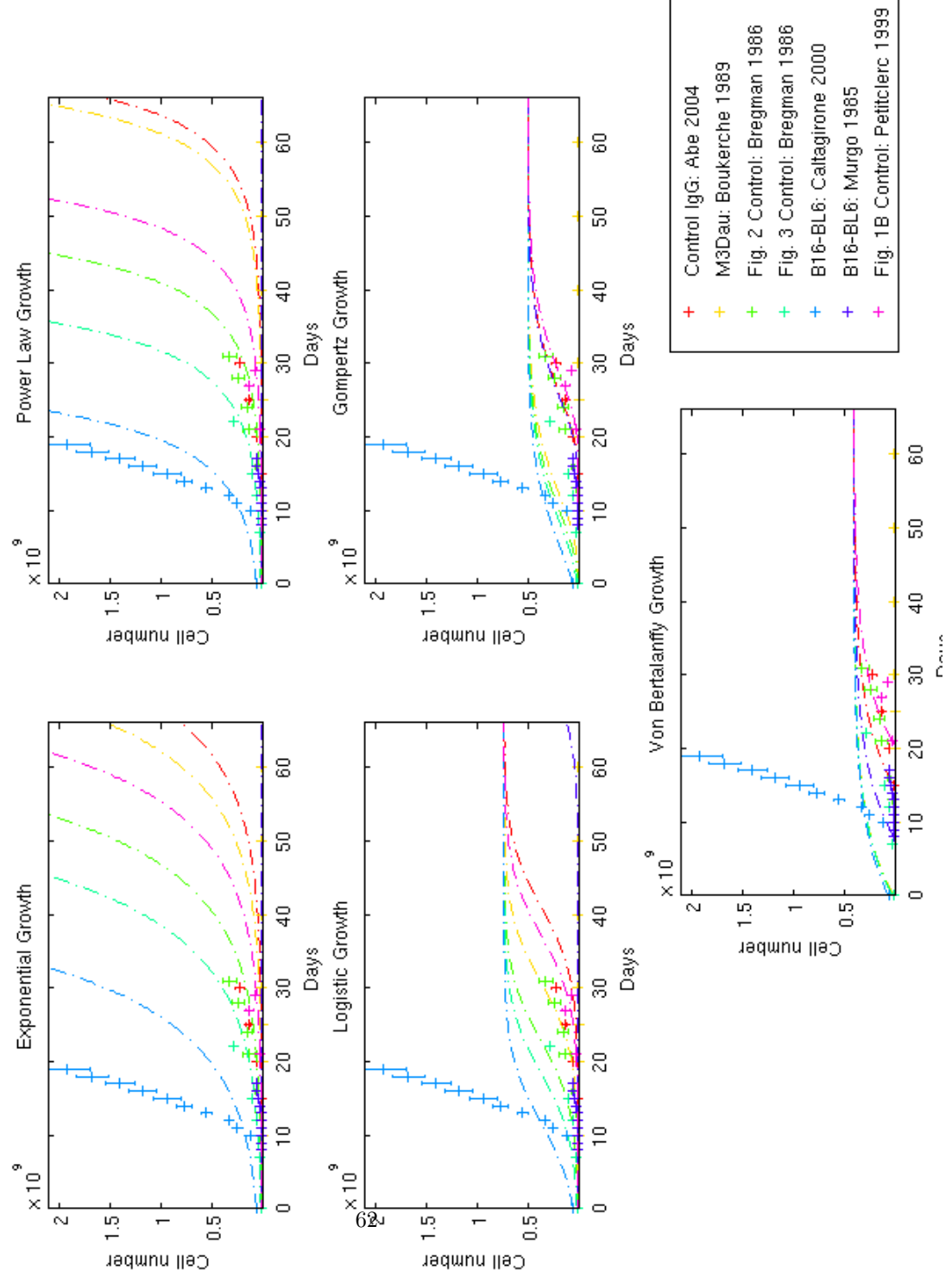


Figure Appendix C.27: Parameter Fitting to Combined *In Vivo* Melanoma Trials

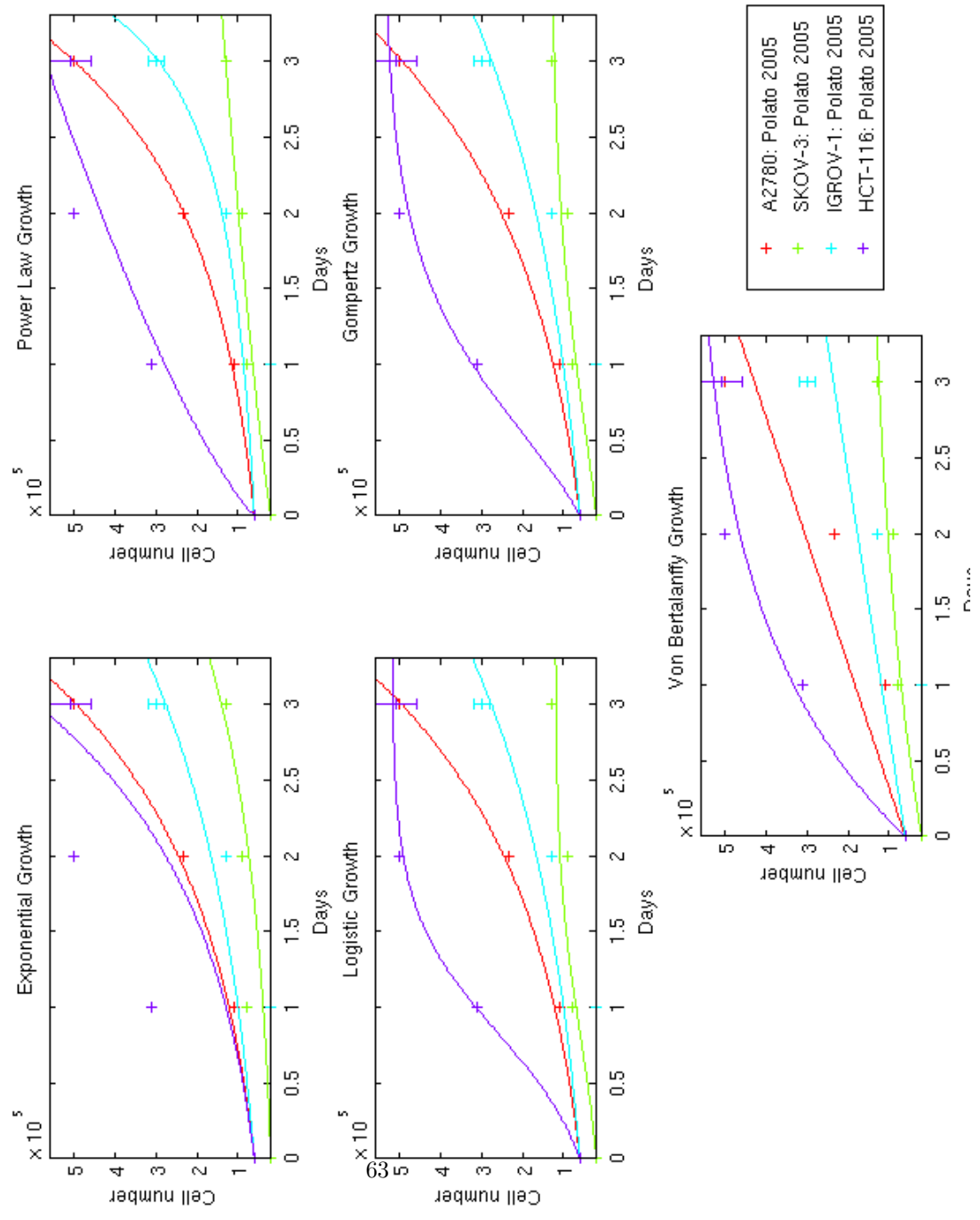


Figure Appendix C.28: Parameter Fittings to Individual *In Vitro* Ovarian Cancer Trials

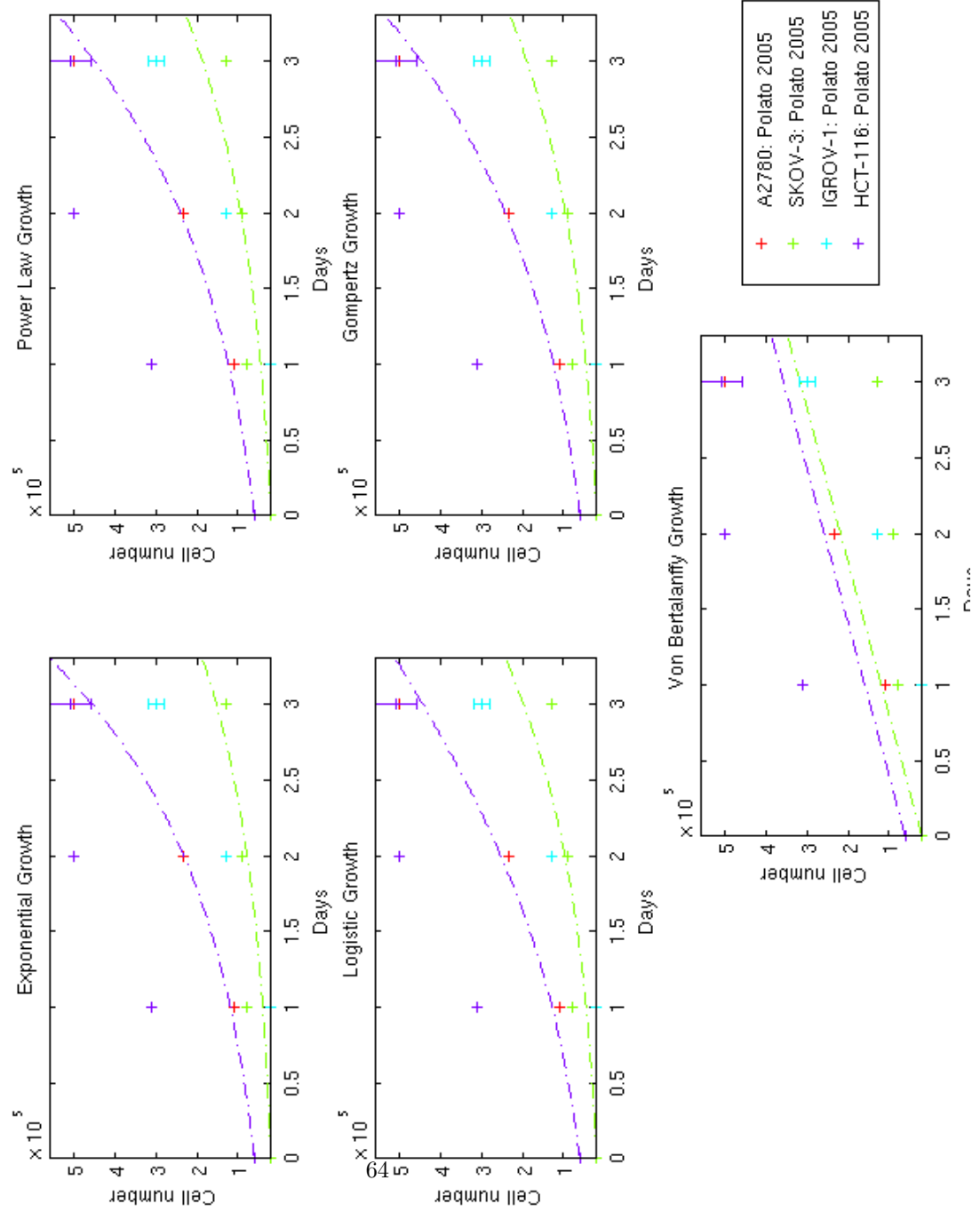


Figure Appendix C.29: Parameter Fitting to Combined *In Vitro* Ovarian Cancer Trials

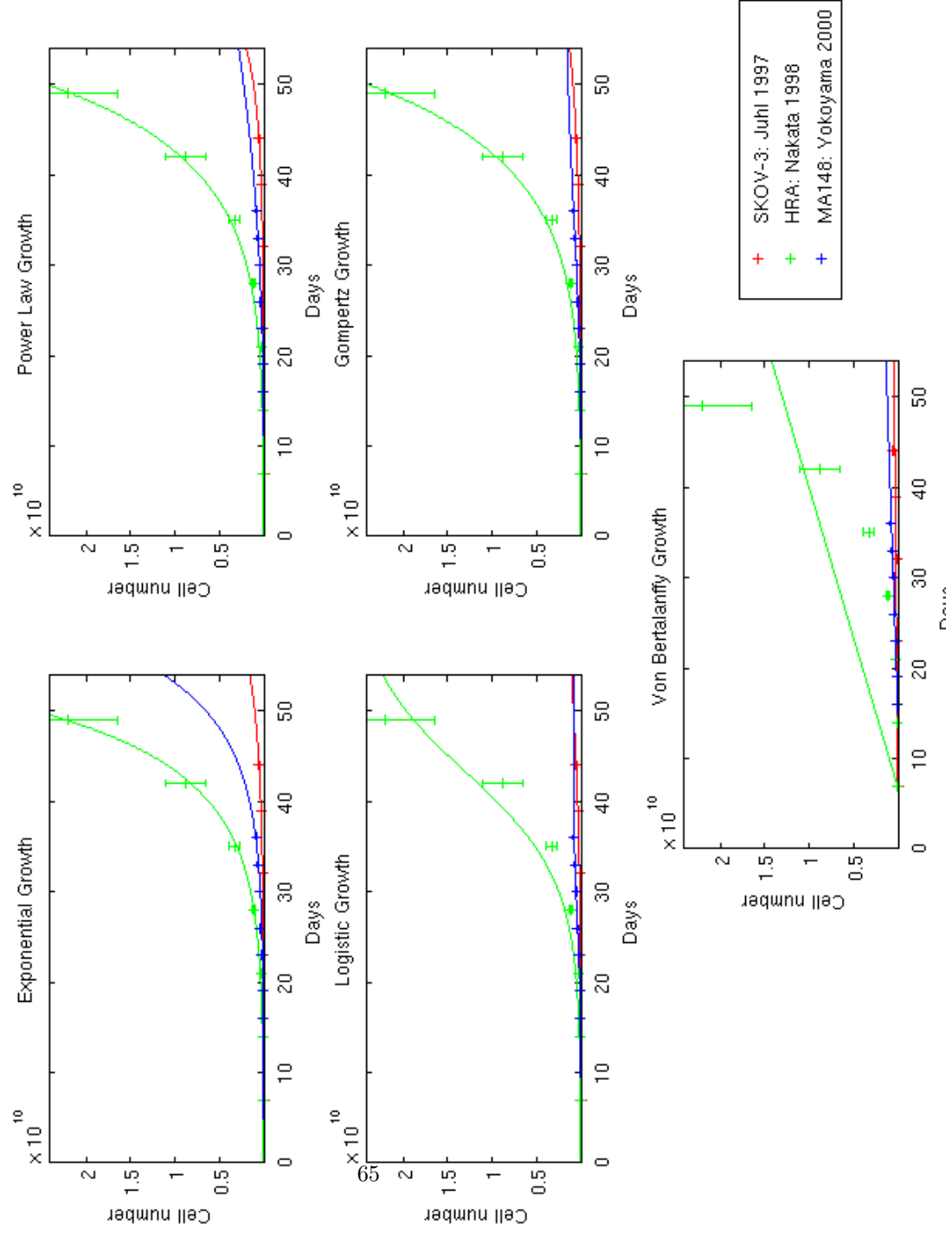


Figure Appendix C.30: Parameter Fittings to Individual *In Vivo* Ovarian Cancer Trials

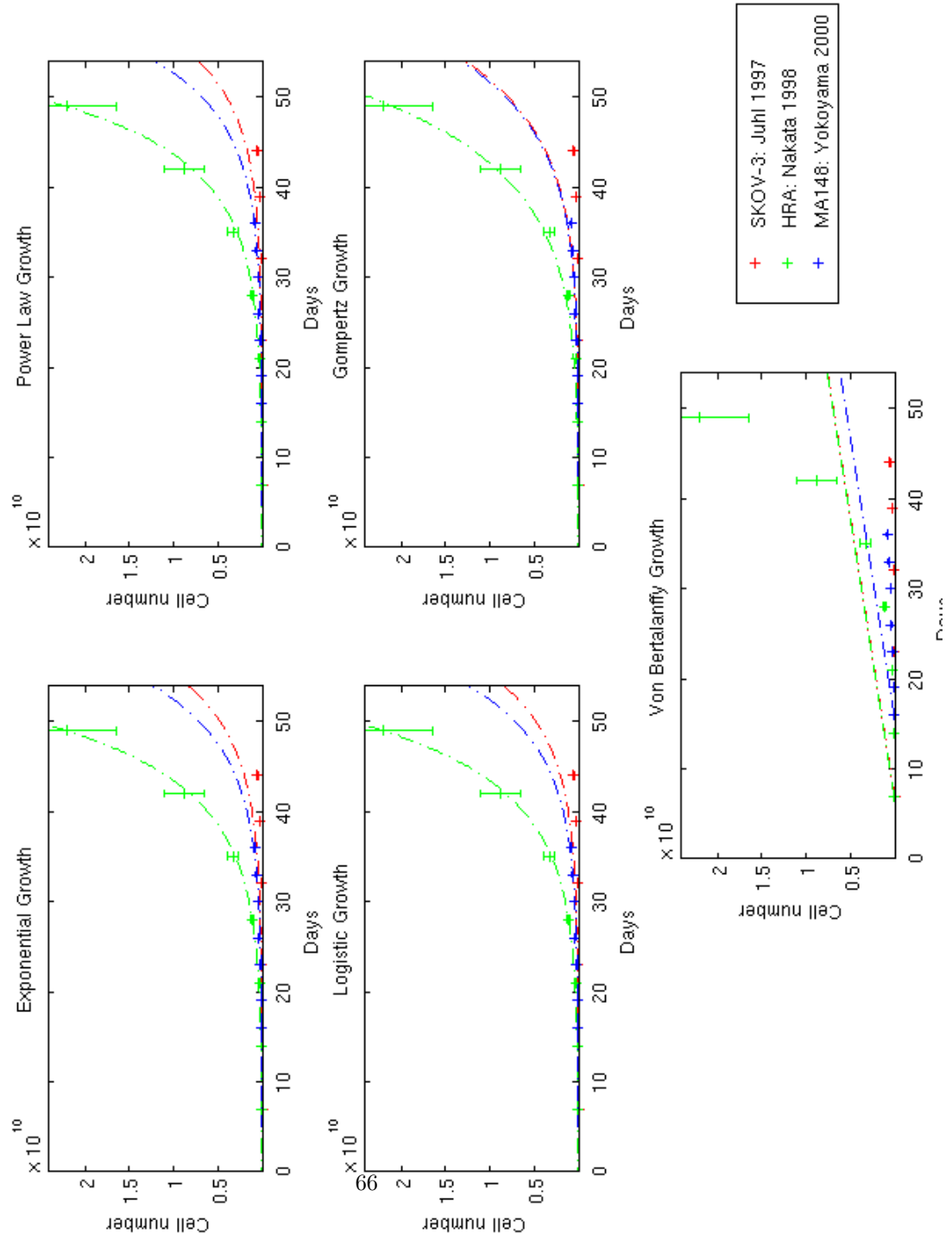


Figure Appendix C.31: Parameter Fitting to Combined *In Vivo* Ovarian Cancer Trials

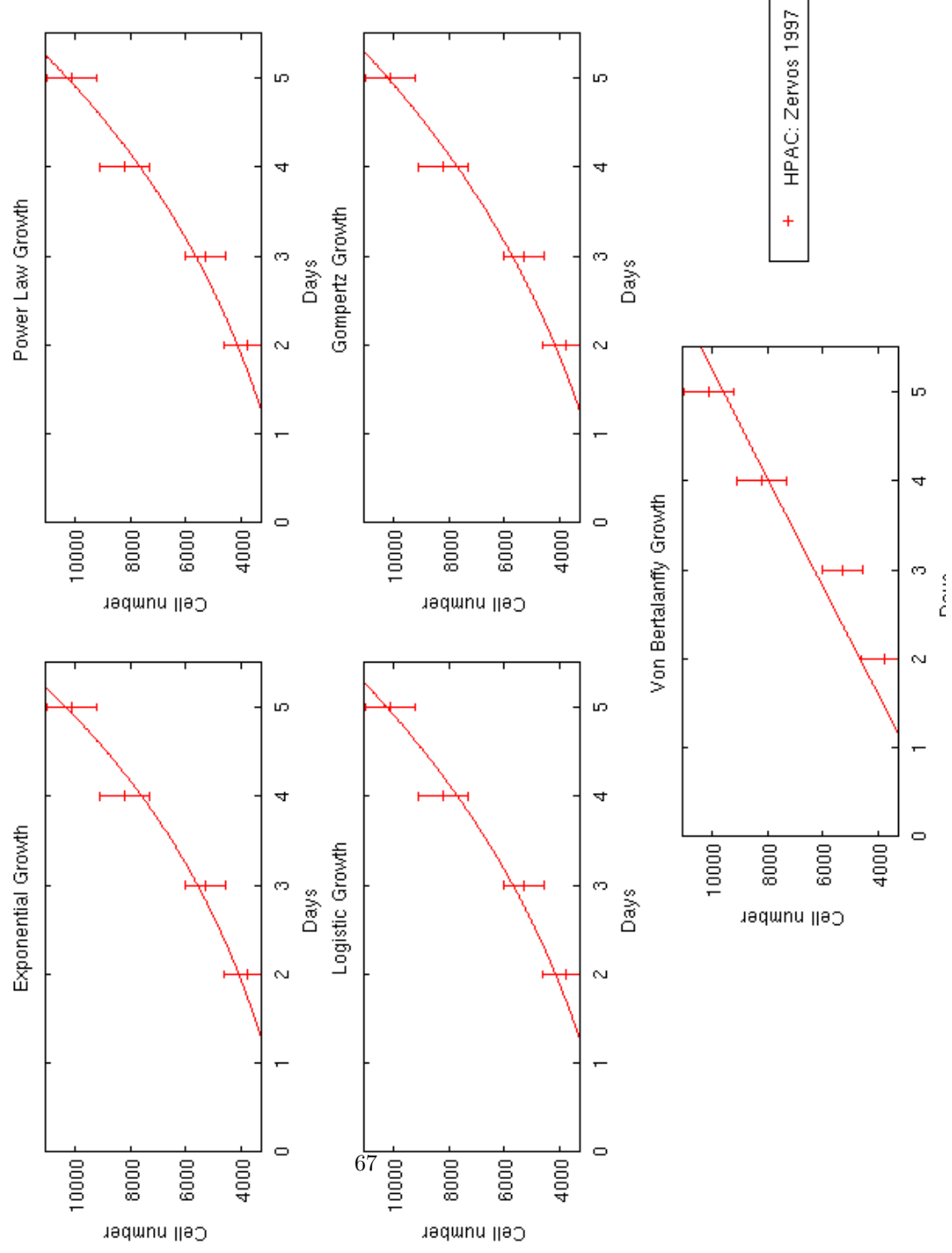


Figure Appendix C.32: Parameter Fittings to *In Vitro* Pancreatic Cancer Trials

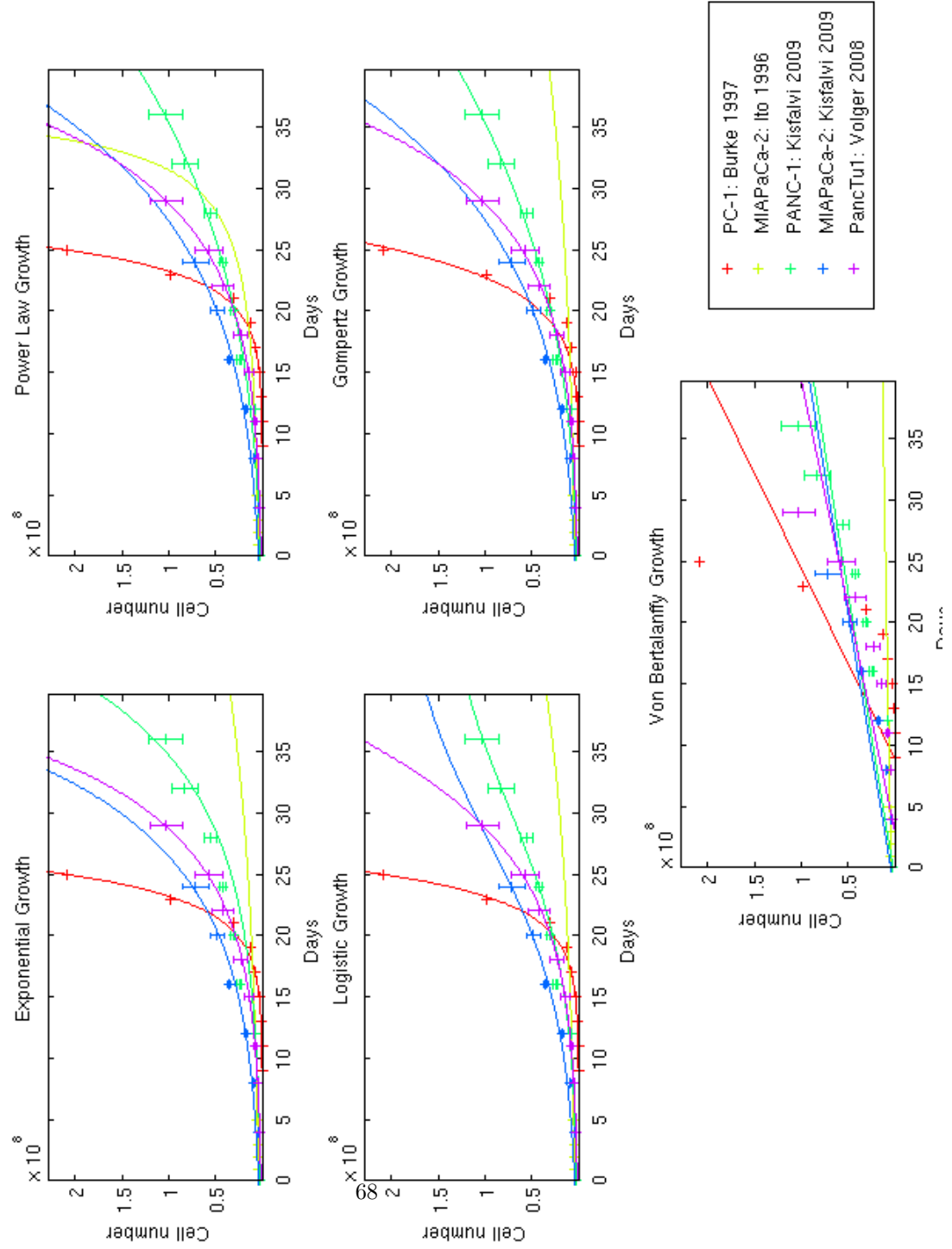


Figure Appendix C.33: Parameter Fittings to Individual *In Vivo* Pancreatic Cancer Trials

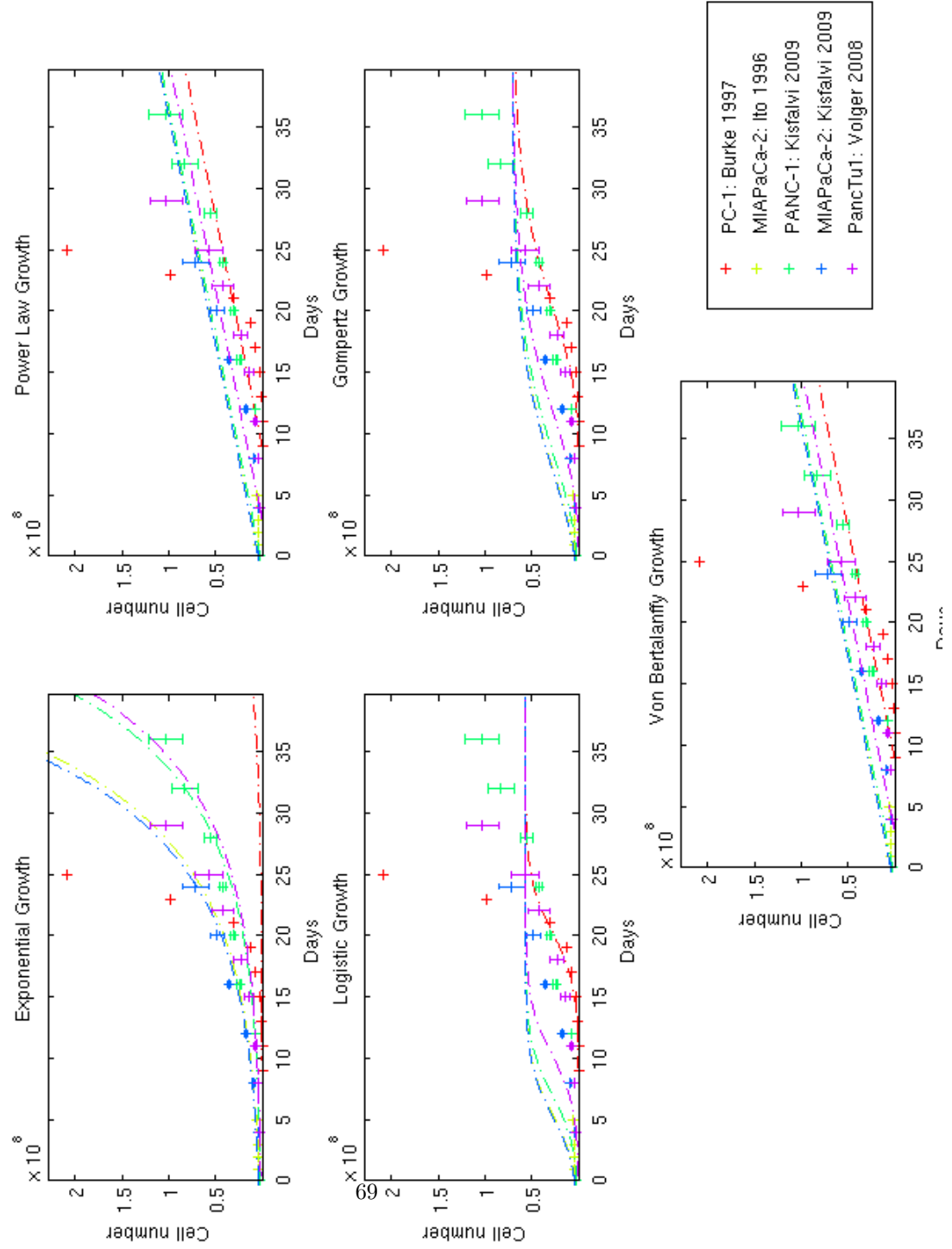


Figure Appendix C.34: Parameter Fitting to Combined *In Vivo* Pancreatic Cancer Trials

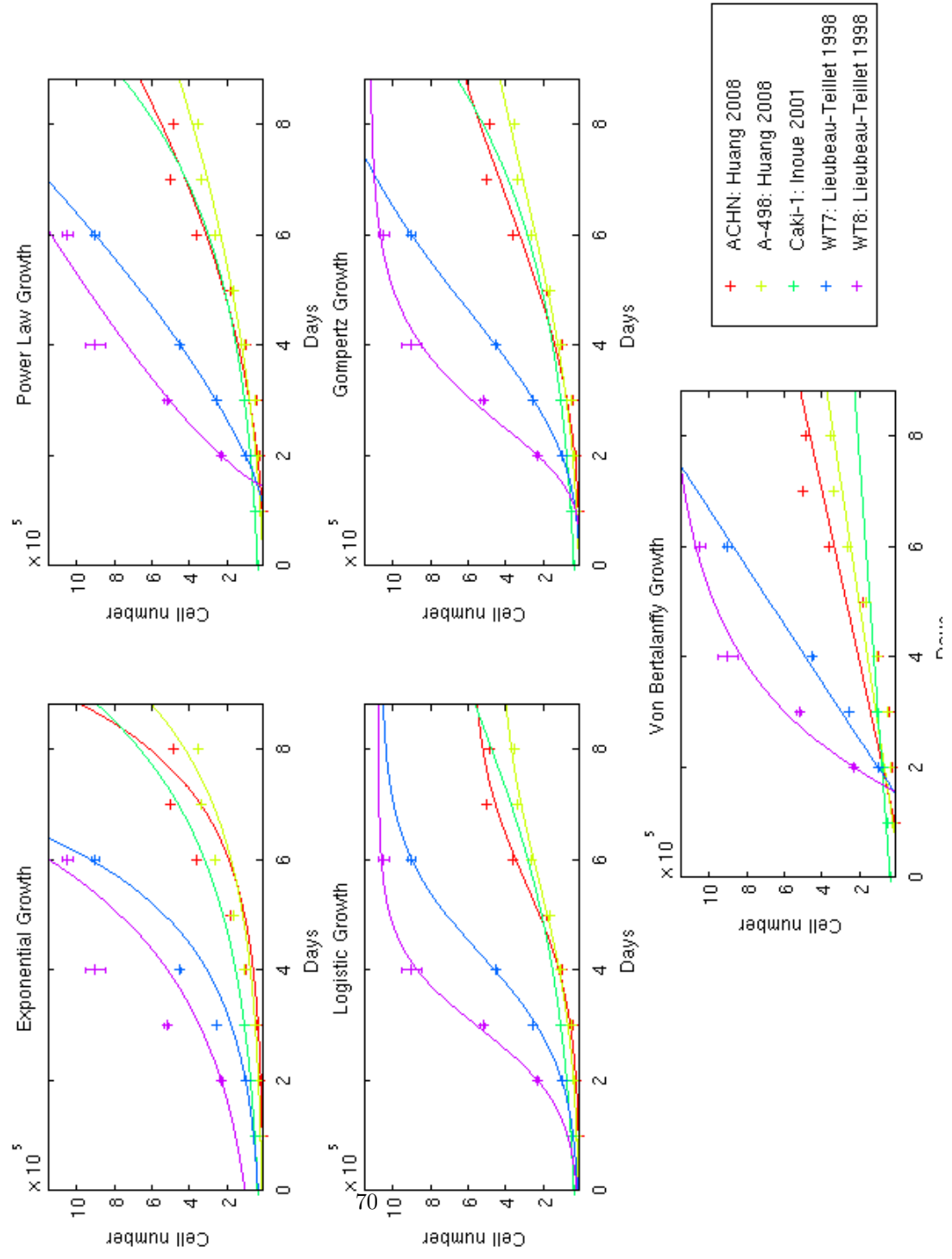


Figure Appendix C.35: Parameter Fittings to Individual *In Vitro* Renal Cell Carcinoma Trials

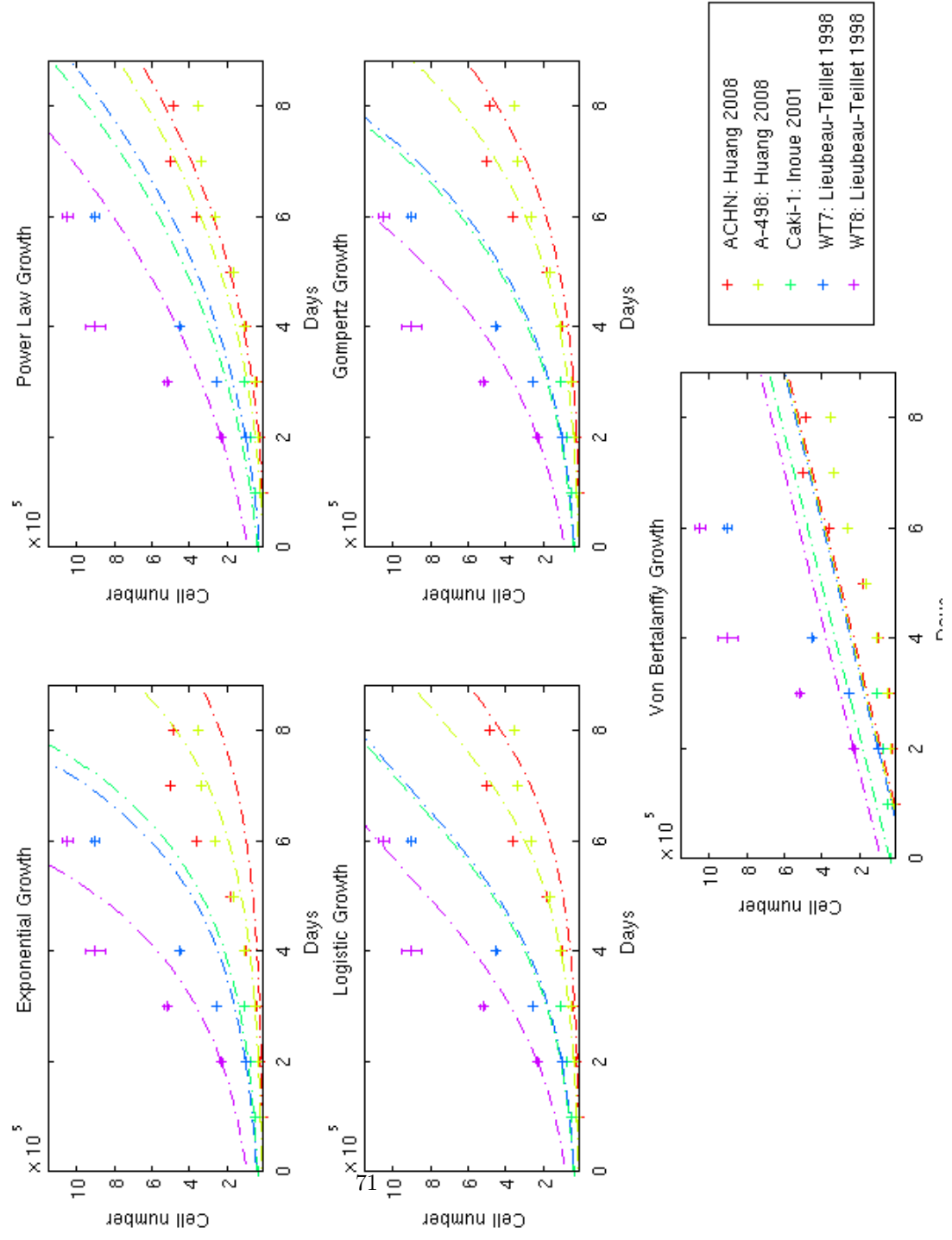


Figure Appendix C.36: Parameter Fitting to Combined *In Vitro* Renal Cell Carcinoma Trials

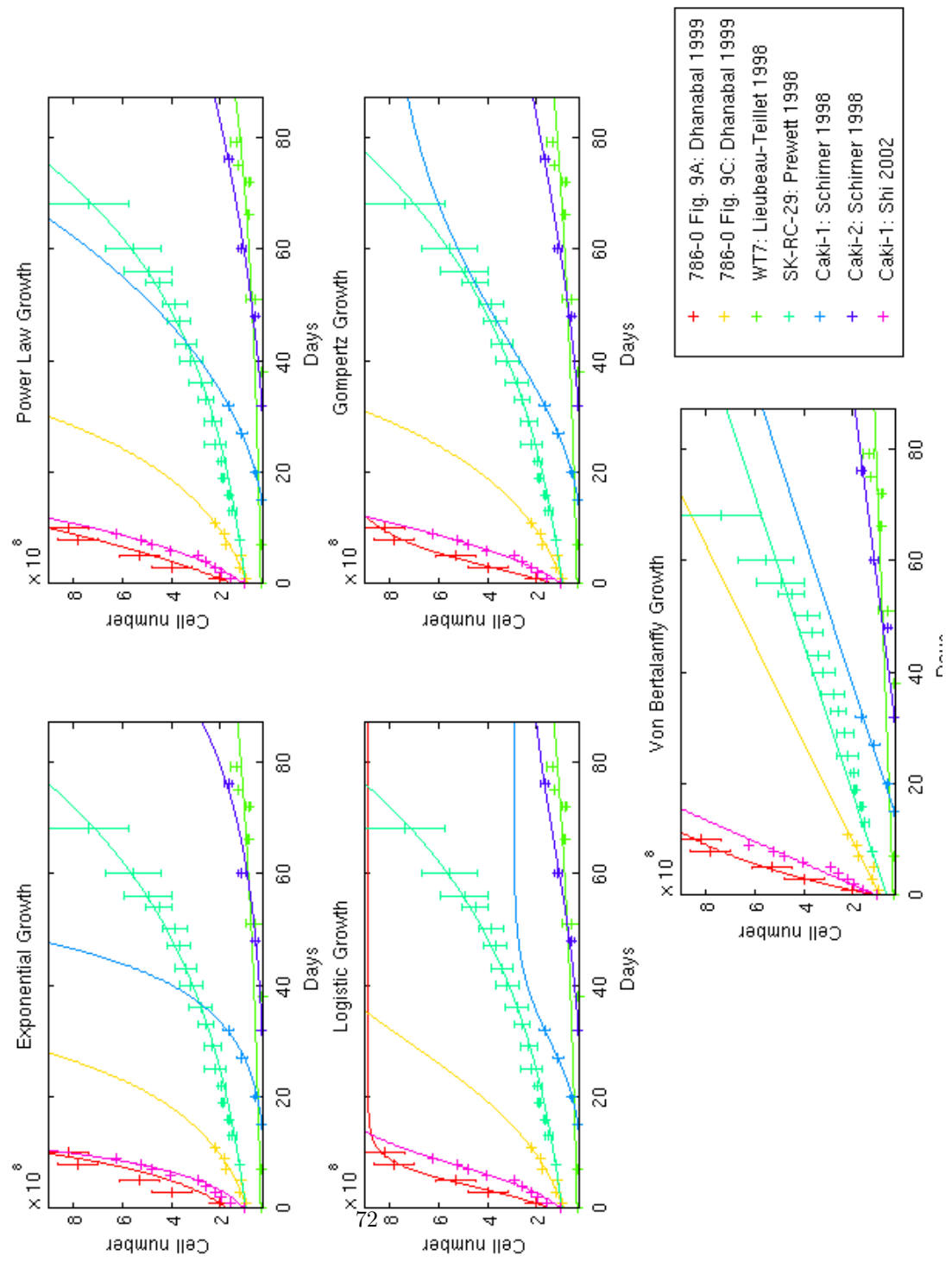


Figure Appendix C.37: Parameter Fittings to Individual *In Vivo* Renal Cell Carcinoma Trials

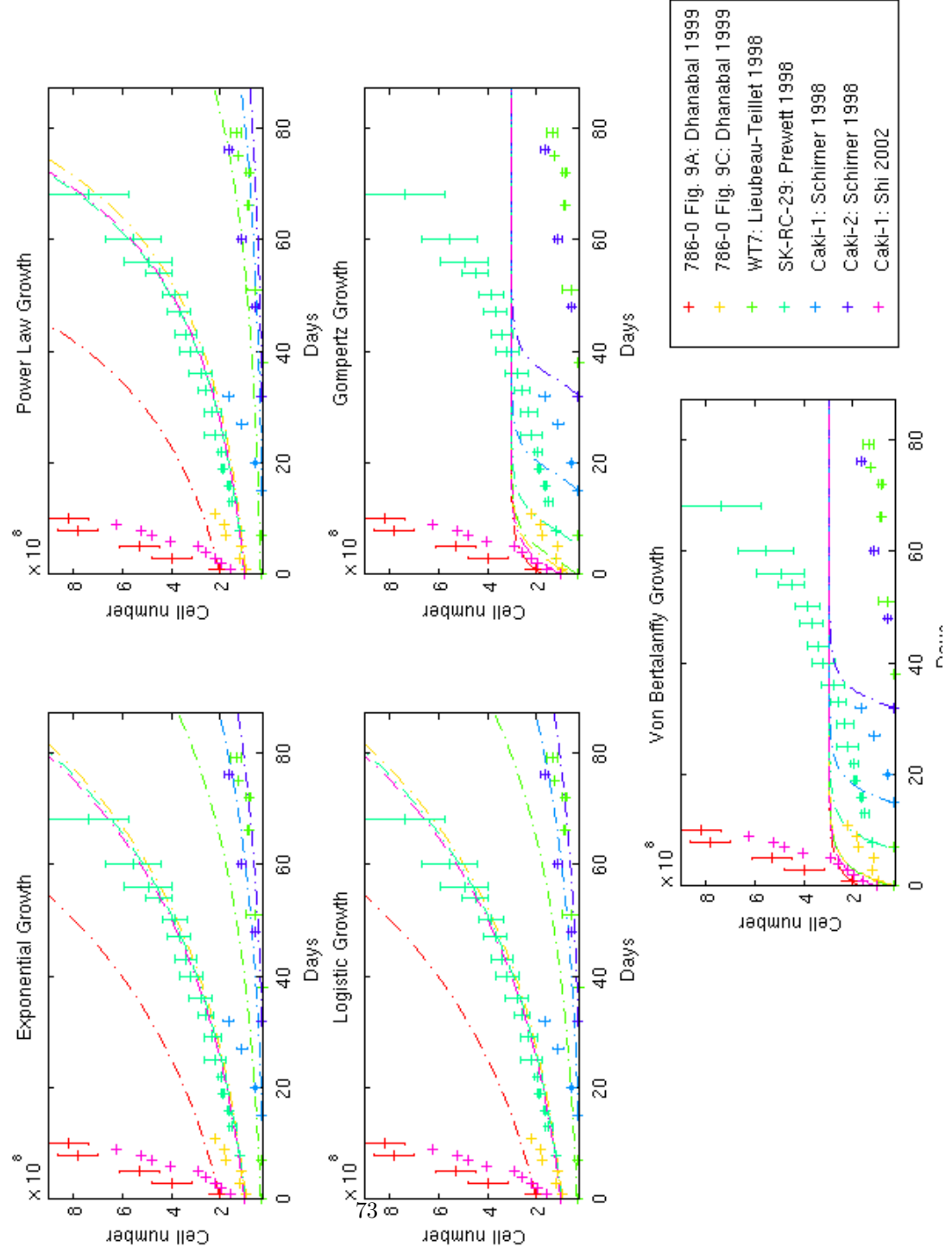


Figure Appendix C.38: Parameter Fitting to Combined *In Vivo* Renal Cell Carcinoma Trials